Structural Synthesis Considering Mixed Discrete-Continuous Design Variables: A Bayesian Framework

H. A. Jensen[1,3], D. J. Jerez[2], and M. Beer[2,3,4]

[1] *Department of Civil Engineering, Federico Santa Maria Technical University, Valparaiso, Chile*

[2] *Institute for Risk and Reliability, Leibniz Universität Hannover, 30167 Hannover, Germany.*

[3] *International Joint Research Center for Engineering Reliability and Stochastic Mechanics, Tongji University, Shanghai 200092, China.*

[4] *Institute for Risk and Uncertainty and School of Engineering, University of Liverpool, Liverpool L69 7ZF, United Kingdom.*

Abstract

In this work attention is directed to general structural optimization problems considering discrete-continuous design variables. The optimization problem is formulated as the minimization of an objective function subject to multiple design requirements. The mathematical programming statement is set into the framework of a Bayesian model updating problem. Constraints are handled directly within the proposed scheme, generating designs distributed over the feasible design space. Based on these samples, a set of designs lying in the vicinity of the optimal solution set is obtained. The Bayesian model updating problem is solved by an effective Markov chain Monte Carlo simulation scheme, where appropriate proposal distributions are introduced for the continuous and discrete design variables. The approach can efficiently estimate the sensitivity of the final design and constraints with respect to the design variables. In addition, the numerical implementation of the optimization algorithm depends on few control parameters. For illustration purposes, the general formulation is applied to an important class of problems, specifically, reliability-based design optimization of structural systems under stochastic excitation. Three numerical examples showing the effectiveness and potentiality of the approach reported herein are presented.

Keywords: Bayesian updating, Discrete-continuous optimization, Feasible design space, Markov sampling method, Reliability-based optimization, Stochastic optimization.

Email addresses: hector.jensen@usm.cl (H. A. Jensen[1,3], D. J. Jerez[2], and M. Beer[2,3,4]), hector.jensen@usm.cl (H. A. Jensen[1,3], D. J. Jerez[2], and M. Beer[2,3,4])

1. Introduction

In a large number of practical design situations some of the design variables must be selected from a list of discrete values. For example, cross-sectional areas of truss, beam and column members usually have to be chosen from a list of commercially available member sizes. Also, the growing use of composite materials underlines the importance of being able to treat structural optimization problems where some or even all of the design variables are discrete. Thus, due to manufacturing limitations the design variables cannot be considered as continuous but should be treated as discrete in a large number cases. Standard optimization procedures involving discrete design variables have been extensively studied in the literature [1, 2, 3]. Methods such as branch and bound techniques, and combinatorial methods treat the discrete variable design optimization problems directly in the primal variable space [4, 5]. Similarly, dual methods have also been used in this context, especially for convex and separable formulations. In these cases, the primal problem can be efficiently solved by dual methods of mathematical programming [6, 7]. The previous methods are rather general and they have been applied in a number of standard optimization problems [5, 8, 9].

Another class of optimization algorithms for solving mixed-discrete constrained optimization problems is based on stochastic search algorithms. A number of stochastic optimization algorithms based on natural mechanisms have been proposed for the purpose of dealing with this class of problems. The most used heuristic techniques include Genetic Algorithms [10, 11, 12, 13], Simulated Annealing [14, 15, 16], and Particle Swarm Optimization [17, 18, 19]. In this context, one important problem is how to handle multiple constraints. Several strategies such as the rejection method, the penalty function method, the constraint fitness priority based ranking method, and the multi-objective function method have been devised for the previous stochastic optimization algorithms [20, 21, 22, 23, 24, 25]. Although the previous algorithms have been applied in a number of mixed-discrete optimization formulations, it is clear that each method has its own definition and formulation as well as specific properties and limitations. Besides, and based on the fact that design optimization is still a challenging problem, there is still room for further developments in this area, specially when dealing with complex structural optimization problems.

In this work, a stochastic search algorithm for mixed discrete-continuous constrained design optimization is developed based on a Bayesian model updating formulation. The proposed approach represents a generalization of the contribution presented in [26] to the case of mixed discrete-

continuous design variables. First, samples (designs) distributed over the feasible design space are generated. Based on these samples, a set of designs lying in the vicinity of the optimal solution set is obtained. The Bayesian model updating problem is solved by an efficient Markov chain Monte Carlo (MCMC) simulation scheme. In particular, the transitional Markov chain Monte Carlo (TMCMC) method is considered [27, 28]. Appropriate proposal distributions, in the context of the Metropolis-Hastings algorithm [29, 30], are suggested for the continuous and discrete design variables. A salient feature of the present work is the development of a population-based stochastic optimization algorithm for solving constrained design optimization problems involving mixed discrete-continuous design variables. The methodology is based on a well-developed and widely employed Bayesian model updating approach and therefore the same framework is adapted for an effective optimization scheme. The proposed solution scheme can efficiently explore the sensitivity of the final design and constraints with respect to the design variables in the neighborhood of the optimal solution set. In addition, the proposed constraint-handling approach is direct and does not require special constraint-handling techniques. Moreover, the optimization algorithm can be implemented with few control parameters. Finally, the proposed general formulation is applied to an important class of problems, specifically, reliability-based design optimization of structural systems subject to stochastic excitation.

The structure of the paper is as follows. In Section 2, the general formulation of the problem is presented. The solution scheme is outlined in detail in Sections 3 and 4. A number of numerical implementation aspects are discussed in Section 5. The scope of application and some benefits of the proposed optimization scheme are addressed in Section 6. The application of the general formulation to reliability-based design optimization of structural systems subject to stochastic excitation is discussed in Section 7. Three numerical examples are presented in Section 8. The paper closes with some final remarks.

2. Optimization Problem

Consider the following structural optimization problem defined as the identification of a vector of design variables $\mathbf{x}$, to minimize an objective function $f(\mathbf{x})$

$$\text{Minimize } f(\mathbf{x}) \tag{1}$$

subject to the design constraints

$$h_j(\mathbf{x}) \leq 1 \ , \quad j = 1, \ldots, n_h \tag{2}$$

which represent the requirements that must be satisfied by the system to give an acceptable design. These constraints can be given in terms of geometric conditions, demand levels, robustness conditions, design specifications characterized by means of different performance measures, etc. Additionally, the system is subject to the side constraints

$$x_{ci}^l \leq x_{ci} \leq x_{ci}^u \ , \quad i = 1, \ldots, n_c \tag{3}$$

and

$$x_{di} \in \mathbf{X}_{di} = \{x_{di(j)}, j = 1, \ldots, n_{di}\} \ , \quad i = 1, \ldots, n_d \tag{4}$$

where $\mathbf{x}_c(x_{ci}, i = 1, \ldots, n_c) \in \mathbf{X}_c \subset R^{n_c}$ denotes the set of continuous design variables, $\mathbf{x}_d(x_{di}, i = 1, \ldots, n_d) \in \mathbf{X}_d \subset R^{n_d}$ denotes the set of discrete design variables, and $\mathbf{x} = \langle \mathbf{x}_c^T, \mathbf{x}_d^T \rangle^T \in \mathbf{X} = \mathbf{X}_c \times \mathbf{X}_d \subset R^{n_c+n_d}$ is the vector of all design or control variables involved in the problem. The constants x_{ci}^l and x_{ci}^u in Eq. (3) are the lower and upper limits for the design variables that are continuous, i.e., $x_{ci}, i = 1, \ldots, n_c$. On the other hand, Eq. (4) represents the side constraints for the design variables that are discrete, i.e., $x_{di}, i = 1, \ldots, n_d$, where the set $\mathbf{X}_{di}$ represents the available discrete values for the i^{th} discrete design variable. Thus, the side constraints characterize physical limitations on the design variables directly in terms of their allowable values. Moreover, the objective function $f(\mathbf{x})$ can be defined in terms of general cost functions or expected performance measures. Therefore, the above formulation is rather general in the sense that different optimization formulations can be considered.

3. Solution Scheme

3.1. Underlying Idea

First, it is noted that finding the minimum of the objective function $f(\mathbf{x})$ is equivalent to find the maximum of the auxiliary function $\exp(-f(\mathbf{x})/T)$, for any given value of $T > 0$ [14]. Next, treating the design variables as random variables uniformly distributed over the feasible design space $\mathbf{X}_{\text{feasible}}$, where

$$\mathbf{X}_{\text{feasible}} = \left\{ \mathbf{x} = \langle \mathbf{x}_c^T, \mathbf{x}_d^T \rangle^T : \mathbf{x}_c \in \mathbf{X}_c \wedge \mathbf{x}_d \in \mathbf{X}_d \wedge \ \ h_j(\mathbf{x}) \leq 1 \ , \ j = 1, \ldots, n_h \right\}, \tag{5}$$

consider the non-normalized auxiliary distribution

$$p_T(\mathbf{x}) \propto \exp\left(-\frac{f(\mathbf{x})}{T}\right) \; I_{\mathbf{X}_{\text{feasible}}}(\mathbf{x}) \tag{6}$$

where $I_{\mathbf{X}_{\text{feasible}}}(\mathbf{x})$ is the indicator function of the feasible design space $\mathbf{X}_{\text{feasible}}$, that is, $I_{\mathbf{X}_{\text{feasible}}}(\mathbf{x}) = 1$, for $\mathbf{x} \in \mathbf{X}_{\text{feasible}}$, and $I_{\mathbf{X}_{\text{feasible}}}(\mathbf{x}) = 0$, otherwise. Based on the previous definition, it is seen that $p_T(\mathbf{x})$ becomes proportional to $I_{\mathbf{X}_{\text{feasible}}}(\mathbf{x})$ as $T \to \infty$. Besides, as $T \to 0$ the distribution $p_T(\mathbf{x})$ becomes spikier, and it puts more and more of its probability mass into the set that maximizes the auxiliary function $\exp(-f(\mathbf{x})/T)$. Thus, a sample drawn from $p_T(\mathbf{x})$ will be in the vicinity of the optimal solution set $\mathbf{X}_f^*$ with a very high probability when $T \to 0$ [31, 32]. In other words, a sample point (design) with smaller value of $f(\mathbf{x})$ has higher probability density function value and the distribution $p_T(\mathbf{x})$ is concentrated in a volume around the optimal solution set $\mathbf{X}_f^*$ when $T \to 0$, i.e., designs having the smallest values of $f(\mathbf{x})$ in the feasible design space. Note that the treatment of the design variables as random variables is just a tool in the present formulation for setting the optimization problem into a Bayesian framework [31, 32, 33].

3.2. Bayesian Framework

Based on the previous ideas, if a number of samples (designs) following the distribution $p_T(\mathbf{x})$ as $T \to 0$ can be generated, then the sample points with the smallest value of $f(\mathbf{x})$ among the generated designs can provide a good approximation for the optimal solution set of the problem. For generating the required samples, a Markov chain Monte Carlo (MCMC) simulation scheme is considered. Markov chain Monte Carlo is a class of algorithms for sampling from target probability distributions that cannot be directly sampled in an efficient manner [34]. These algorithms are based on the construction of Markov chains that have the distribution of interest as its stationary distribution. In this context, the conventional Metropolis-Hastings (MH) algorithm [29, 30], one of the most popular MCMC techniques, has proved to be quite general but it may encounter some difficulties. One of the difficulties includes the proper definition of the proposal distribution so that the acceptance rate of the candidate state is not too small to avoid highly repetitive samples, and at the same time so that the optimal solution set is effectively explored. One of the consequences of using the direct MH algorithm is that the convergence rate of the stationary distribution of the state to the target distribution may be very slow. In this regard, the transitional Markov chain Monte Carlo method (TMCMC) provides a good alternative for sampling from the target

probability distribution $p_T(\mathbf{x})$ as $T \to 0$ [27, 35]. The TMCMC method has proved to be quite effective in a number of Bayesian model updating problems [27, 36, 37, 38, 39].

3.3. Basic TMCMC Implementation

In the framework of the TMCMC method, define a sequence of non-normalized intermediate distributions as

$$p_{T_0}(\mathbf{x}) \propto I_{\mathbf{X}_{\text{feasible}}}(\mathbf{x}) \tag{7}$$

$$p_{T_j}(\mathbf{x}) \propto \exp\left(-\frac{f(\mathbf{x})}{T_j}\right) I_{\mathbf{X}_{\text{feasible}}}(\mathbf{x}) \quad , \quad j = 1, 2, \ldots \tag{8}$$

where $\infty = T_0 > T_1 > \ldots > T_j > \ldots$ is a sequence of monotonically decreasing parameters with $T_j \to 0$ as $j \to \infty$. In the context of the original TMCMC implementation for Bayesian model updating, the design variables $\mathbf{x}$ correspond to the model parameters to be updated, the function $I_{\mathbf{X}_{\text{feasible}}}(\mathbf{x})$ represents the non-normalized prior distribution, the function $\exp(-f(\mathbf{x}))$ takes the role of the likelihood function, and $p_{T_j}(\mathbf{x})$ is the posterior distribution as $T_j \to 0$ [33]. Note that the corresponding prior normalized distribution is the uniform distribution, $U_{\mathbf{X}_{\text{feasible}}}(\mathbf{x})$, defined over the feasible design space. In the first step, the samples (designs) $\mathbf{x}_1^0, \ldots, \mathbf{x}_n^0$ are generated from the prior distribution $U_{\mathbf{X}_{\text{feasible}}}(\mathbf{x})$ in order to populate the feasible design space. The samples at stage $j+1$, i.e. $\mathbf{x}_1^{j+1}, \ldots, \mathbf{x}_n^{j+1}$, $j = 0, 1, \ldots$, are obtained by generating Markov chains using the Metropolis-Hastings algorithm. It is noted that the candidate sample should belong to the feasible design space. If not, the sample is rejected. Otherwise, the standard acceptance/rejection test is applied to the generated sample. The parameters $T_j, j = 1, 2, \ldots$ are constructed adaptively in such a way that the distributions $p_{T_j}(\mathbf{x})$ and $p_{T_{j+1}}(\mathbf{x})$ be similar. To this end, different criteria can be used [27, 40, 41]. This small change of the shape between consecutive distributions allows to efficiently obtain samples from $p_{T_{j+1}}(\mathbf{x})$ based on the samples from $p_{T_j}(\mathbf{x})$. The procedure is repeated until a stopping criterion is satisfied. The idea of the method is to iterate until the parameter T_{j+1} is small enough so that the corresponding samples $\mathbf{x}_1^{j+1}, \ldots, \mathbf{x}_n^{j+1}$ are distributed over the optimal solution set $\mathbf{X}_f^*$. In fact, due to the annealing property of the TMCMC method, the samples at the last stage, that is, when $T_j \to 0$, tend to maximize the likelihood function and therefore minimize the objective function $f(\mathbf{x})$. The reader is referred to [27, 28, 35] for a detailed implementation of the TMCMC method.

3.4. MH Proposal Distribution

In the context of the Metropolis-Hastings algorithm, the candidate sample (design) $\mathbf{x}^*$ is drawn from a proposal distribution q. Generally, the proposal distribution can be symmetric, i.e. $q(\mathbf{x}^*|\tilde{\mathbf{x}}) = q(\tilde{\mathbf{x}}|\mathbf{x}^*)$, where $\tilde{\mathbf{x}}$ is the current state or lead sample, asymmetric, i.e. $q(\mathbf{x}^*|\tilde{\mathbf{x}}) \neq q(\tilde{\mathbf{x}}|\mathbf{x}^*)$, or an independent sampler, i.e. $q(\mathbf{x}^*|\tilde{\mathbf{x}}) = q(\mathbf{x}^*)$. For the independent sampler (global proposal) to work well, the proposal distribution must be a good approximation of the target distribution, otherwise a large fraction of the candidate samples will be rejected and the Markov chain will be too slow in covering the important regions of the target distribution. Such a proposal is usually difficult to construct in practical cases. On the other hand, when the proposal distribution is of the form $q(\mathbf{x}^*|\tilde{\mathbf{x}})$ (local proposal) it is less sensitive to the target distribution, and therefore this option, which is more frequently used than global proposals, is considered in the present formulation. In this work, the proposal distribution is written in terms of two independent distributions, one related to the continuous design variables and the other one associated with the discrete design variables. The description of the proposal distributions is given in Sections 5.2 and 5.3.

4. Procedure

4.1. Constraint Handling

Based on the proposed solution scheme, it is observed that a set of samples distributed over the feasible design space $\mathbf{X}_{\text{feasible}}$ is required at the first stage. Such samples (designs) must verify the side constraints, i.e., $\mathbf{x}_c \in \mathbf{X}_c$, $\mathbf{x}_d \in \mathbf{X}_d$, and the design constraints $h_j(\mathbf{x}) \leq 1, j = 1, \ldots, n_h$. Following the ideas suggested in [26], the samples confined in the feasible design space can be generated as follows. First, define an auxiliary optimization problem of the form

$$\text{Minimize } g(\mathbf{x}) \tag{9}$$

with side constraints

$$x_{ci}^l \leq x_{ci} \leq x_{ci}^u \quad , \quad i = 1, \ldots, n_c \tag{10}$$

and

$$x_{di} \in \mathbf{X}_{di} = \{x_{di(j)}, j = 1, \ldots, n_{di}\} \quad , \quad i = 1, \ldots, n_d \tag{11}$$

where the objective function $g(\mathbf{x})$ is taken as

$$g(\mathbf{x}) = \begin{cases} \max_{j=1,\ldots,n_h} \{h_j(\mathbf{x})\} & \text{if } \exists\ j : h_j(\mathbf{x}) > 1 \\ 1 & \text{if } \forall\ j\ ,\ h_j(\mathbf{x}) \leq 1 \end{cases} \tag{12}$$

Note that the above optimization problem is unconstrained in the sense that only side constraints on the design variables are considered. It is observed that the corresponding optimal solution set $\mathbf{X}_g^*$ is given by

$$\mathbf{X}_g^* = \left\{ \mathbf{x} = \langle \mathbf{x}_c^T, \mathbf{x}_d^T \rangle^T : \mathbf{x}_c \in \mathbf{X}_c \wedge \mathbf{x}_d \in \mathbf{X}_d \wedge h_j(\mathbf{x}) \leq 1\ ,\ j = 1, \ldots, n_h \right\} \tag{13}$$

where the minimum value of the objective function $g(\mathbf{x})$ is equal to one. Thus, as it can be seen by comparing Eqs. (5) and (13), the optimal solution set $\mathbf{X}_g^*$ of the unconstrained optimization problem provides a set of samples in the feasible design space, that is, $\mathbf{X}_{\text{feasible}} = \mathbf{X}_g^*$.

4.2. Samples in the Feasible Design Space

The required designs in the feasible design space can be obtained by the proposed solution scheme (see Section 3.3) where the sequence of non-normalized intermediate distributions is redefined as

$$p_{T_0}(\mathbf{x}) \propto\ U_{\mathbf{X}}(\mathbf{x}) \tag{14}$$

$$p_{T_j}(\mathbf{x}) \propto\ \exp\left(-\frac{g(\mathbf{x})}{T_j}\right)\ U_{\mathbf{X}}(\mathbf{x})\ \ ,\ \ j = 1, 2, \ldots \tag{15}$$

where $U_{\mathbf{X}}(\mathbf{x})$ is the uniform distribution defined over the set that characterizes the side constraints, i.e., $\mathbf{X} = \{\mathbf{x} = \langle \mathbf{x}_c^T, \mathbf{x}_d^T \rangle^T : \mathbf{x}_c \in \mathbf{X}_c \wedge \mathbf{x}_d \in \mathbf{X}_d\}$. Note that for the case of discrete design variables, each available value has equal probability to be observed during the first stage ($j = 0$). According to the proposed solution scheme, the samples at the last stage of the process ($T_j \to 0$) represent possible designs with similar minimum values of the objective function $g(\mathbf{x})$. Consequently, such samples constitute the sought feasible designs, as previously pointed out. Moreover, all feasible samples generated during the different stages of the procedure are uniformly distributed over the feasible design space. Note that the feasible designs are obtained in the framework of the solution scheme outlined in the previous section. Therefore, special constraint-handling techniques are not necessary.

In addition, it is noted that the feasible samples generated from the sequence of distributions defined in Eqs. (14) and (15) can be used for exploring the feasible design space. At the same time, the information from the generated samples can be used for evaluating and estimating the interaction between the different design variables in the feasible design space. Such information can give important insight into the optimization problem. Moreover, the feasible samples can be used in the context of other optimization algorithms. For example, the best design among the generated samples can be used as the initial design for a given optimizer.

4.3. Samples in the Optimal Solution Set

Once the set of feasible designs has been generated, the procedure outlined in Section 3.3 is used to iteratively generate samples following the distributions defined in Eq. (8). The samples tend to be distributed over the optimal solution set $\mathbf{X}_f^*$, as indicated before. If a single final design is needed, a reasonable choice is the design with the smallest objective function value among the samples in the optimal solution set. In other words, $\mathbf{x}^* = arg\ min_{i=1,\ldots,n} f(\mathbf{x}_i^{j+1})$, where the designs $\mathbf{x}_i^{j+1}, i = 1, \ldots, n$ are the samples at the last stage of the process. Note that the proposed procedure does not require the use of the so-called move-limits for the design variables. The procedure directly updates the important region in the feasible design space that contains a significant portion of the intermediate distribution probability mass during the updating process.

5. Numerical Implementation Aspects

5.1. Updating Implementation

The proposed updating process for the continuous design variables is performed in an underlying normal space $\mathbf{Y}_c \subset R^{n_c}$ of independent standard normal variables rather than in the physical space $\mathbf{X}_c$. In fact, validation calculations have shown that performing the updating process in the underlying standard normal space has some numerical advantages due to normalization and boundedness issues [28, 33]. The mapping between the spaces $\mathbf{Y}_c$ and $\mathbf{X}_c$, that is, $\mathbf{x}_c = \mathbf{x}_c(\mathbf{y}_c)$ is given by $x_{ci} = x_{ci}(y_{ci}) = x_{ci}^l + \Phi(y_{ci})(x_{ci}^u - x_{ci}^l), i = 1, \ldots, n_c$, where $\Phi(\cdot)$ is the standard normal cumulative univariate distribution function. Nonetheless, a direct implementation of the updating process in the physical design space of the continuous design variables is also possible. On the other hand, additional calculations have indicated that it is more convenient to perform the sample generation process for the discrete design variables directly in the physical space of the design variables, i.e., $\mathbf{X}_d$ [42].

5.2. Proposal Distribution: Continuous Design Variables

A symmetric proposal distribution q_c is considered for the continuous design variables. At stage $j+1$, and based on the sampling spaces outlined in Section 5.1, the proposal is taken as a Gaussian distribution centered at the current state or lead sample $\tilde{\mathbf{y}}_c^{j+1}$, and with covariance matrix $\mathbf{\Sigma}_j$ equal to a scaled version of the estimate covariance matrix of the current marginal intermediate distribution p_{T_j}, that is,

$$\mathbf{\Sigma}_j = \beta^2 \sum_{i=1}^{n} \bar{w}_i^j \left(\mathbf{y}_{ci}^j - \bar{\mathbf{y}}_c^j\right)\left(\mathbf{y}_{ci}^j - \bar{\mathbf{y}}_c^j\right)^T \tag{16}$$

where $\mathbf{y}_{ci}^j, i = 1,\ldots,n$ are the samples at stage j in the underlying standard normal space, $\bar{\mathbf{y}}_c^j = \sum_{i=1}^n \bar{w}_i^j \mathbf{y}_{ci}^j$, β is a scaling parameter, and $\bar{w}_i^j$ is the normalized importance weight of the sample involving all design variables, that is, $\langle \mathbf{y}_{ci}^{j^T}, \mathbf{x}_{di}^{j^T}\rangle^T, i = 1,\ldots,n$. The normalized importance weight is given by $\bar{w}_i^j = w_i^j / \sum_{p=1}^{n} w_p^j, \quad i = 1,\ldots,n$, where w_i^j is the corresponding importance weight of the sample $\langle \mathbf{y}_{ci}^{j^T}, \mathbf{x}_{di}^{j^T}\rangle^T$. The sample importance weight is equal to

$$w_i^j = \exp\left(-g(\mathbf{x}_i^j)\left[\frac{1}{T_{j+1}} - \frac{1}{T_j}\right]\right), \quad i = 1,\ldots,n \tag{17}$$

for the step that generates feasible samples, and

$$w_i^j = \exp\left(-f(\mathbf{x}_i^j)\left[\frac{1}{T_{j+1}} - \frac{1}{T_j}\right]\right), \quad i = 1,\ldots,n \tag{18}$$

for the step producing samples distributed in the vicinity of the optimal solution set, where $\mathbf{x}_i^j = \langle \mathbf{x}_c(\mathbf{y}_{ci}^j)^T, \mathbf{x}_{di}^{j^T}\rangle^T$. The scaling parameter β can be defined directly by the user, or it can be determined by an adaptive scheme that monitors the acceptance rate during the updating process [28, 43]. Note that the current state vector $\langle \tilde{\mathbf{y}}_c^{j+1^T}, \tilde{\mathbf{x}}_d^{j+1^T}\rangle^T$ is a sample from stage j that is selected according to a probability equal to the normalized importance weight of the samples $\langle \mathbf{y}_{ci}^{j^T}, \mathbf{x}_{di}^{j^T}\rangle^T, i = 1,\ldots,n$. The candidate sample generated by the previous distribution is denoted by $\mathbf{y}_c^*$.

5.3. Proposal Distribution: Discrete Design Variables

5.3.1. Definition

The proposal distribution q_d for the vector of discrete design variables $\mathbf{x}_d$ is defined in terms of independent proposal distributions corresponding to each discrete variable in the physical design space, that is,

$$q_d(\mathbf{x}_d^*|\tilde{\mathbf{x}}_d^{j+1}) = \prod_{l=1}^{n_d} q_{dl}(x_{dl}^*|\tilde{x}_{dl}^{j+1}) \tag{19}$$

where $\mathbf{x}_d^* = \langle x_{d1}^*, \ldots, x_{dn_d}^* \rangle^T$ is the candidate sample, $\tilde{\mathbf{x}}_d^{j+1} = \langle \tilde{x}_{d1}^{j+1}, \ldots, \tilde{x}_{dn_d}^{j+1} \rangle^T$ is the current state or lead sample of the discrete design variables at stage $j+1$ as indicated before, and $q_{dl}(x_{dl}^*|\tilde{x}_{dl}^{j+1})$ is the proposal distribution for the discrete variable x_{dl}. The candidate sample x_{dl}^* is selected from the set of discrete values adjacent to $\tilde{x}_{dl}^{j+1}$, including the current state value. This set is denoted by $Adj(\tilde{x}_{dl}^{j+1})$, and it is defined as

$$Adj(\tilde{x}_{dl}^{j+1}) = \{x_{dl(i)_{i=1,\ldots,n_{di}}} : \lambda(\tilde{x}_{dl}^{j+1}, x_{dl(i)}) \leq \lambda_l^*\} \tag{20}$$

where $\lambda(\tilde{x}_{dl}^{j+1}, x_{dl(i)})$ is the *distance* between the lead sample $\tilde{x}_{dl}^{j+1}$ and the sample $x_{dl(i)}$. If the lead sample corresponds to the s^{th} available value of the discrete variable x_{dl}, that is, $\tilde{x}_{dl}^{j+1} = x_{dl(s)}$, then the distance between these two samples is defined as

$$\lambda(\tilde{x}_{dl}^{j+1}, x_{dl(i)}) = \lambda(x_{dl(s)}, x_{dl(i)}) = |s - i| \tag{21}$$

Recall that the available discrete values for the discrete design variables are listed in an ascending order. To allow for the possibility to consider a nonadjacent value of $\tilde{x}_{dl}^{j+1}$, a small probability τ of randomly selecting a nonadjacent value is considered. Note that the chance of moving to a nonadjacent value is independent of the current state value $\tilde{x}_{dl}^{j+1}$. Based on the previous ideas, the proposal distribution for the l^{th} discrete design variable is defined as

$$q_{dl}(x_{dl}^*|\tilde{x}_{dl}^{j+1}) = \begin{cases} \frac{1-\tau}{Card(Adj(\tilde{x}_{dl}^{j+1}))} & \text{if } x_{dl}^* \in Adj(\tilde{x}_{dl}^{j+1}) \\ \frac{\tau}{Card(Adj^c(\tilde{x}_{dl}^{j+1}))} & \text{if } x_{dl}^* \notin Adj(\tilde{x}_{dl}^{j+1}) \end{cases} \tag{22}$$

where $Card(Adj(\tilde{x}_{dl}^{j+1}))$ is the number of discrete available values in the set $Adj(\tilde{x}_{dl}^{j+1})$, $Adj^c(\tilde{x}_{dl}^{j+1})$ is the complement set of $Adj(\tilde{x}_{dl}^{j+1})$, and $Card(Adj^c(\tilde{x}_{dl}^{j+1}))$ is the number of discrete available values which are not adjacent to $\tilde{x}_{dl}^{j+1}$.

5.3.2. Distribution Parameters

Clearly, the value of the distribution parameters λ_l^* and τ is problem-dependent. They can be selected directly by the user or they can be modified by an adaptive scheme that monitors the acceptance rate during the updating process. In this regard, a number of schemes can be devised. It is noted that the parameter λ_l^* is related to the definition of the support of the proposal distribution. Generally, if this parameter is *large*, the probability to accept a new candidate state is relatively low and this results in a chain remaining still for long periods of time. On the other hand, if the parameter is *small* the chain explores the state space very slowly. Thus, the selection of this parameter has an important impact on the speed of convergence of the Markov chain to its stationary distribution. In terms of the parameter τ, validation calculations carried out in the context of the present work have shown that a value $\tau \leq 0.1$ is adequate for the proposed procedure that generates samples in the feasible design space. Moreover, for the proposed scheme that generates samples in the vicinity of the optimal solution set, a small value is recommended. Generally, if this is not the case, the acceptance rate during the corresponding updating process tends to decrease, and therefore the scheme becomes less efficient. Specific values for the distribution parameters are provided in the numerical examples.

5.4. Acceptance/Rejection Test

Considering the sampling spaces for the design variables indicated before, the acceptance/rejection test, in the context of the MH algorithm, is implemented as follows. The candidate sample that includes all design variables, i.e, $\langle \mathbf{y}_c^{*T}, \mathbf{x}_d^{*T} \rangle^T$ is accepted with probability ρ^* given by

$$\rho^* = Min \left\{ 1, \frac{\exp\left(-g(\mathbf{x}^*)/T_{j+1}\right)}{\exp\left(-g(\tilde{\mathbf{x}}^{j+1})/T_{j+1}\right)} \frac{\pi(\mathbf{y}_c^*)}{\pi(\tilde{\mathbf{y}}_c^{j+1})} \frac{q_d(\tilde{\mathbf{x}}_d^{j+1}|\mathbf{x}_d^*)}{q_d(\mathbf{x}_d^*|\tilde{\mathbf{x}}_d^{j+1})} \right\} \tag{23}$$

for the step that generates feasible samples, and

$$\rho^* = Min \left\{ 1, I_{\mathbf{X}_{\text{feasible}}}(\mathbf{x}^*) \frac{\exp\left(-f(\mathbf{x}^*)/T_{j+1}\right)}{\exp\left(-f(\tilde{\mathbf{x}}^{j+1})/T_{j+1}\right)} \frac{\pi(\mathbf{y}_c^*)}{\pi(\tilde{\mathbf{y}}_c^{j+1})} \frac{q_d(\tilde{\mathbf{x}}_d^{j+1}|\mathbf{x}_d^*)}{q_d(\mathbf{x}_d^*|\tilde{\mathbf{x}}_d^{j+1})} \right\} \tag{24}$$

for the step that generates samples in the vicinity of the optimal solution set. In the previous expressions, $\mathbf{x}^* = \langle \mathbf{x}_c(\mathbf{y}_c^*)^T, \mathbf{x}_d^{*T} \rangle^T$, $\tilde{\mathbf{y}}_c^{j+1}$ is the current state of the continuous design variables represented in the standard normal space as previously pointed out, $\pi(\cdot)$ is the multivariate standard normal probability density function associated with the underlying normal space $\mathbf{Y}_c$, and all other

terms have been previously defined. Moreover, according to the definition of the discrete proposal distribution, the ratio $q_d(\tilde{\mathbf{x}}_d^{j+1}|\mathbf{x}_d^*)/q_d(\mathbf{x}_d^*|\tilde{\mathbf{x}}_d^{j+1})$ is given by

$$\frac{q_d(\tilde{\mathbf{x}}_d^{j+1}|\mathbf{x}_d^*)}{q_d(\mathbf{x}_d^*|\tilde{\mathbf{x}}_d^{j+1})} = \prod_{l=1}^{n_d} \begin{cases} \frac{Card(Adj(\tilde{x}_{dl}^{j+1}))}{Card(Adj(x_{dl}^*))} & \text{if } x_{dl}^* \in Adj(\tilde{x}_{dl}^{j+1}) \\ \frac{Card(Adj^c(\tilde{x}_{dl}^{j+1}))}{Card(Adj^c(x_{dl}^*))} & \text{if } x_{dl}^* \notin Adj(\tilde{x}_{dl}^{j+1}) \end{cases} \tag{25}$$

If the candidate state $\langle \mathbf{y}_c^{*T}, \mathbf{x}_d^{*T} \rangle^T$ is rejected, the current sample $\langle \tilde{\mathbf{y}}_c^{j+1^T}, \tilde{\mathbf{x}}_d^{j+1^T} \rangle^T$ is repeated. For completeness and self-containment, schematic flowcharts for generating samples in the feasible design space and samples in the optimal solution set are provided in Appendices A and B, respectively [26].

6. Scope of Proposed Procedure

It is noted that due to the generality and flexibility of the proposed formulation, it can handle, in principle, different types of optimization problems. From the structural point of view, these problems may include complex linear and nonlinear systems, disjoint feasible design spaces, multiple optima, as well as problems involving noisy objective or constraint functions (noisy optimization problems), e.g., general performance-based design optimization problems. Additional potential benefits of using the proposed optimization scheme include the following. First, the methodology produces a set of nearly optimal solutions instead of a single optimal solution. This feature can be advantageous in many practical cases where alternative criteria can be taken into account to select the appropriate final design. Thus, the approach provides flexibility to the decision-making process. Second, the scheme is a useful tool for exploration of complex feasible design spaces, which is especially useful when design variables exhibit a complex interaction between them. Third, valuable sensitivity information is provided by the approach. In fact, sensitivity of the feasible designs and the final design with respect to the design variables can be obtained directly. Fourth, the algorithm does not require special constraint-handling techniques. Actually, samples in the feasible design space are obtained from the solution of an unconstrained optimization problem which is directly defined in terms of the constraint functions of the original problem. Moreover, the same framework for obtaining samples in the vicinity of the optimal solution set is used for solving the unconstrained optimization problem. This feature is an advantage from a practical viewpoint. Finally, the technique is very-well suited for parallel implementation in a computer cluster, which is very important when dealing with optimization problems involving expensive function evaluations.

7. Application to Structural Systems under Stochastic Excitation

As previously pointed out, due to the generality of the proposed formulation, a number of structural optimization problems can be considered. In this regard, an important class of problems is considered within the context of this work. Specifically, reliability-based design optimization of structural systems subject to stochastic excitation. In this framework, design constraints can be characterized by means of different performance measures, such as reliability measures. In fact, for systems under stochastic excitation the probability that design conditions are satisfied within a particular reference period t_T provides a useful reliability measure. Such measure is referred to as the first excursion probability and quantifies the plausibility of the occurrence of unacceptable behavior (failure) of the structural system [44, 45]. The failure domain Ω_F corresponding to a failure event F can be characterized in terms of a demand function d as $\Omega_F(\mathbf{x}) = \{\mathbf{z} \mid d(\mathbf{x}, \mathbf{z}) > 1\}$ where the demand function is defined as

$$d(\mathbf{x}, \mathbf{z}) = \max_{i=1,\ldots,l} \max_{t \in [0,t_T]} \frac{|r^i(t, \mathbf{x}, \mathbf{z})|}{r^{i*}} \tag{26}$$

where $\mathbf{z} \in \mathbf{Z} \subset R^{n_z}$ is the vector of uncertain parameters involved in the problem, $r^i(t, \mathbf{x}, \mathbf{z}), i = 1, \ldots, l$, are the response functions associated with the failure event F, and $r^{i*} > 0$ is the acceptable response level for the response r^i. The responses $r^i, i = 1, \ldots, l$ are functions of time (due to the dynamic nature of the excitation), the design variable vector $\mathbf{x}$, and the random vector $\mathbf{z}$. These responses are obtained from the solution of the equation of motion that characterizes the structural model. Given a design $\mathbf{x}$, the corresponding probability of failure $P_F(\mathbf{x})$ can be expressed in terms of the probability integral

$$P_F(\mathbf{x}) = \int_{\Omega_F(\mathbf{x})} p(\mathbf{z}) d\mathbf{z} \tag{27}$$

where $p(\mathbf{z})$ is the probability density function of the vector of uncertain parameters. This function indicates the relative plausibility of the possible values of the uncertain parameters $\mathbf{z} \in \mathbf{Z}$. Generally, the previous probability integral involves a large number of uncertain parameters (hundreds or thousands)[46, 47, 48]. Therefore, the reliability estimation for a given design constitutes a high-dimensional problem which is usually estimated by advanced simulation techniques. The corresponding reliability constraint, say the j^{th} design constraint, can be written as

$$h_j(\mathbf{x}) = \frac{P_{F_j}(\mathbf{x})}{P^*_{F_j}} \leq 1 \tag{28}$$

where $P_{F_j}(\mathbf{x})$ is a failure probability function, and $P^*_{F_j}$ is the corresponding target failure probability. Finally, it is noted that the design objective can also be defined in terms of expected performance measures such as the system reliability. In this case, the objective function becomes the failure probability function, that is, $f(\mathbf{x}) = P_F(\mathbf{x})$.

8. Illustrative Examples

Three numerical examples are presented in this section. In the first example, the minimization of the system reliability of a simple linear structural model is considered. The second example comprises the reliability-based design of a two-story frame structure equipped with friction-based devices. Finally, the third example deals with the design of a three-dimensional non-linear structural model under reliability constraints related to stress and displacement responses. The objective of the first two examples is to explore in detail the performance of the proposed scheme in a rather didactical manner by means of relatively simple structural models. Moreover, the goal of the third example is to apply the optimization scheme in an application problem that deals with a somewhat involved three-dimensional structural model.

8.1. Example No. 1

A simple structural model which is a lumped mass supported by a column is considered in the first example. The model is shown in Fig. 1, where m ($m = 1$) is the mass of the system, ξ is the damping ratio, k is the stiffness coefficient, and $u(t)$ is the displacement relative to the base.

The system is subjected to a base acceleration modeled as a non-stationary stochastic process. In particular, a stochastic model based on a point-source model is considered [49, 50]. The model is characterized by a sequence of white noise and a series of parameters such as radiation pattern, shear wave velocity in the vicinity of the source, corner frequencies, local site conditions, velocity pulse parameters, and additional seismicity parameters such as the moment magnitude and rupture distance. Details of the procedure can be found in [49, 50, 51, 52]. The base acceleration can be written as $\ddot{u}_g(t, \mathbf{z})$, where $\mathbf{z} \in R^{n_z}$ is the vector of uncertain parameters involved in the characterization of the stochastic excitation model. The objective of the design problem is to minimize the system failure probability with respect to the stiffness and damping coefficients.

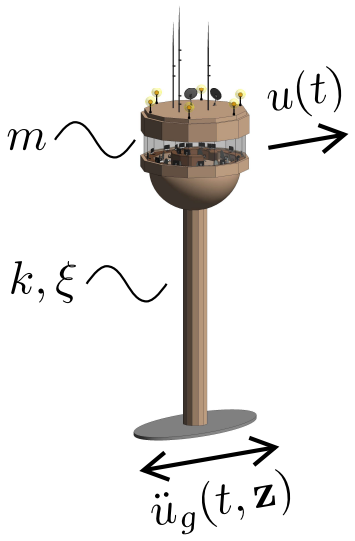

Figure 1: Single-degree-of-freedom system.

The stiffness parameter is treated as a discrete design variable where the available discrete values are given by the set $\mathbf{K} = \{1 + 0.4j, j = 0, 1, \ldots, 10\}$. Thus, the discrete set $\mathbf{K}$ has 11 components. Moreover, the damping ratio is considered as a continuous design variable with side constraints $0.02 \leq \xi \leq 0.1$. Then, the design problem is stated as

$$\begin{aligned} \text{Min}_{\mathbf{x}} \quad & P_F(\mathbf{x}) \\ s.t. \quad & 0.02 \leq \xi \leq 0.1 \\ & k \in \mathbf{K} \end{aligned} \tag{29}$$

where $\mathbf{x} = \langle \xi, k \rangle^T$ is the vector of design variables. In terms of the system failure probability, two design scenarios are considered. In the first scenario, the response of interest is the absolute acceleration $\ddot{u}(t, \mathbf{x}, \mathbf{z}) + \ddot{u}_g(t, \mathbf{z})$, and therefore the normalized demand function is given by

$$d(\mathbf{x}, \mathbf{z}) = \max_{t \in [0, t_T]} \{ \mid \ddot{u}(t, \mathbf{x}, \mathbf{z}) + \ddot{u}_g(t, \mathbf{z}) \mid / \ddot{u}^* \} \tag{30}$$

with an acceptable response level equal to $\ddot{u}^* = 0.55$. In the second scenario, two responses are simultaneously considered for defining the failure event, namely, the absolute acceleration $\ddot{u}(t, \mathbf{x}, \mathbf{z}) + \ddot{u}_g(t, \mathbf{z})$ and the displacement relative to the base $u(t, \mathbf{x}, \mathbf{z})$. The corresponding normalized demand function is written as

$$d(\mathbf{x}, \boldsymbol{\theta}) = \max_{t\in[0,t_T]}\{\mid \ddot{u}(t, \mathbf{x}, \mathbf{z}) + \ddot{u}_g(t, \mathbf{z}) \mid /\ddot{u}^*, \mid u(t, \mathbf{x}, \mathbf{z}) \mid /u^*\} \tag{31}$$

with acceptable response levels $\ddot{u}^* = 0.85$, and $u^* = 0.33$. These values have been calibrated during preliminary calculations in order to obtain a significant interaction between the design variables while maintaining acceptable computational efforts. The duration of the excitation is taken as $t_T = 10$s, with a sampling interval equal to 0.01s. Based on these values and according to the stochastic excitation model under consideration, it can be shown that more than 1000 random variables are involved in the generation of base acceleration samples [46, 49]. Therefore, the reliability estimation for a given design constitutes a high-dimensional problem.

8.1.1. Results of First Scenario

The iso-probability curves in the continuous design space are shown in Figure 2 for reference purposes. These curves are constructed by using a set of failure probability estimates distributed over the design space. The estimates are obtained by averaging the estimates of 10 independent Subset simulation runs with 1000 samples per stage [46, 56]. The resulting curves have been smoothed for presentation purposes. The figure shows a relatively weak interaction between the design variables. Thus, the system reliability is mostly controlled by the stiffness parameter. In addition, it is observed that the smallest failure probabilities are located at the upper-left corner of the design space. That is, the system reliability is maximized for more flexible and more damped designs, which is compatible from a structural point of view.

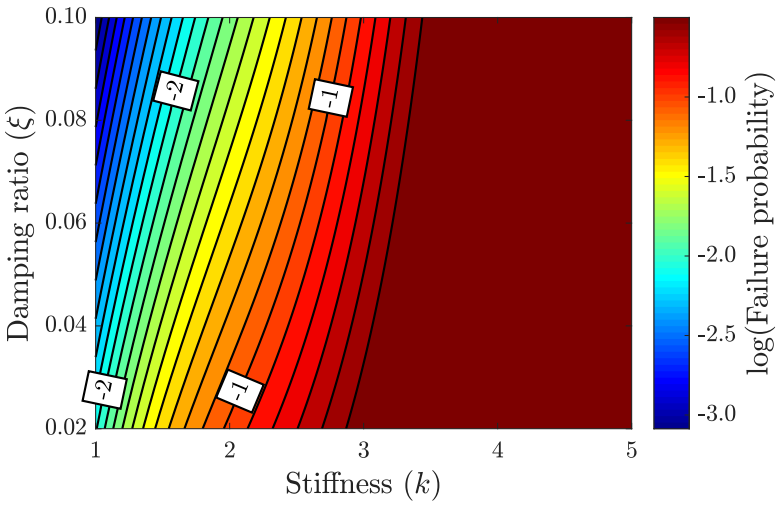

Figure 2: Iso-probability curves. Example No.1: First scenario

Figure 3 shows the samples obtained during the different stages of the design process. The number of samples per stage is equal to 100. The distribution parameters of the proposal distribution for the discrete design variable are set equal to $\lambda_1^* = 1$, and $\tau = 0$. With this selection of λ_1^*, $Card(Adj(\cdot))$ is equal to 3 except when the lead sample takes the lowest or highest value of the available values. In that case, $Card(Adj(\cdot))$ is equal to 2. It is noted that in this problem, the initial set of feasible designs can be obtained directly by Monte Carlo simulation since only side constraints for the design variables are involved in the optimization problem. Thus, there is no need to solve the auxiliary optimization problem defined by Eqs. (9) to (12). After a number of stages the samples populate the vicinity of the optimal design. The corresponding objective function values, i.e., failure probabilities, obtained at each stage are presented in Fig. 4. For convenience, they are sorted in a decreasing manner. At the last stage, the failure probability ranges from 4.02×10^{-4} to 4.19×10^{-4}. Thus, the minimum value obtained during the updating process (sample-based minimum failure probability) is equal to 4.02×10^{-4}, which is associated with the design $k = 1.0$ and $\xi = 0.099$ (sample-based optimum design). It is noted that the previous results correspond to a single optimization run.

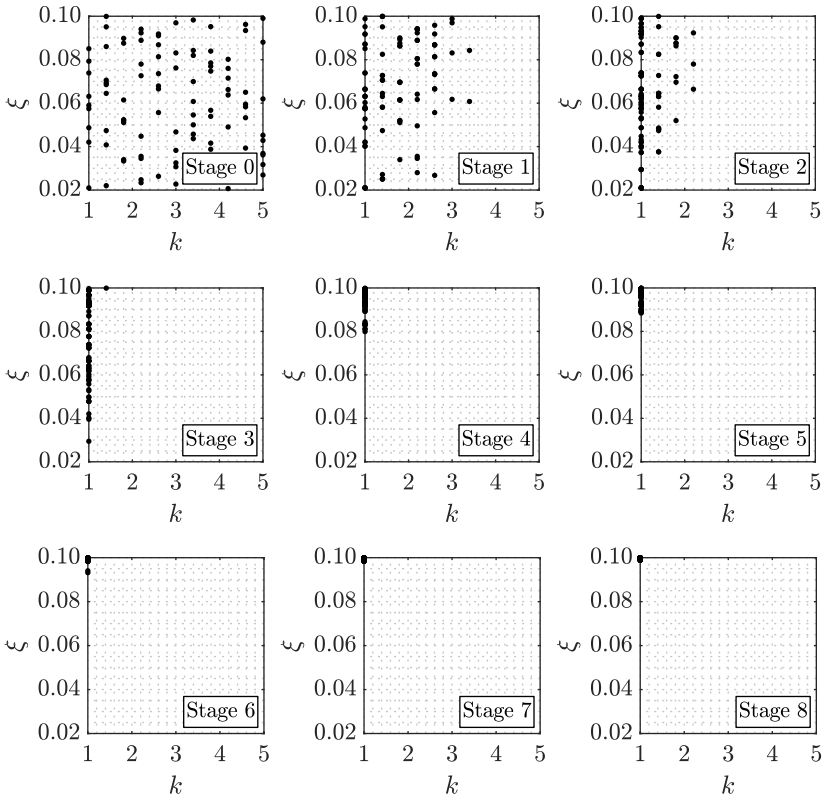

Figure 3: Evolution of samples during different stages. Example No.1: First scenario

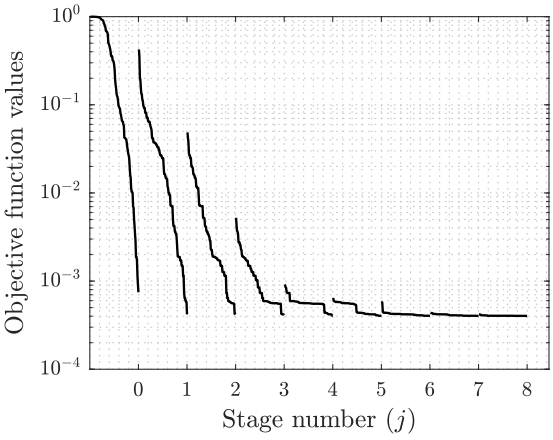

Figure 4: Objective function values obtained during the updating process. Example No.1: First scenario

The performance of the proposed optimization scheme in terms of the number of samples per stage, n, is summarized in Table 1. The statistical performance assessment is based on 30 independent runs of the optimization process. For each run, the sample-based minimum failure probability, that is, the minimum value of the failure probability function across all its stages, is obtained. Based on the 30 independent solutions generated by the proposed method, the corresponding best, mean and worst values as well as the corresponding coefficient of variation, in terms of the system failure probability, are reported in the table. The number of samples per stage ranges from 10 to 200, and the total number of stages is taken equal to 9 (including the initial stage). It can be seen that the best, the mean, and the worst solutions remain almost invariant when the number of samples is greater than 50. Moreover, as expected, the coefficient of variation of the minimum failure probability values obtained in different runs tends to decrease as n increases, and more significantly when n is small. Therefore, the scheme is able to explore the design space in a very effective manner, even with a relatively small number of samples per stage. A different interpretation of this result is that the proposed scheme, which is based on Markov chain simulation, shows a good performance in terms of its ergodicity in this example problem.

8.1.2. Results of Second Scenario

Results of the second scenario are presented in the following figures. Figure 5 shows the iso-probability curves in the continuous design space. As in the previous case, these curves are constructed by using a set of failure probability estimates distributed over the continuous design space. A complex interaction between the design variables is observed in this scenario. This is due to the nature of the response functions considered in the definition of the failure event. The

n	best	mean	worst	c.o.v.
10	4.02×10^{-4}	5.74×10^{-4}	22.36×10^{-4}	8.0×10^{-1}
25	4.02×10^{-4}	4.18×10^{-4}	5.59×10^{-4}	1.0×10^{-1}
50	4.02×10^{-4}	4.03×10^{-4}	4.04×10^{-4}	2.0×10^{-3}
100	4.02×10^{-4}	4.02×10^{-4}	4.03×10^{-4}	1.0×10^{-3}
200	4.02×10^{-4}	4.02×10^{-4}	4.03×10^{-4}	0.5×10^{-3}

Table 1: Statistical performance of proposed scheme. Example No.1: First scenario

designs that minimize the failure probability lie in a region associated with intermediate stiffness values and highest damping ratios.

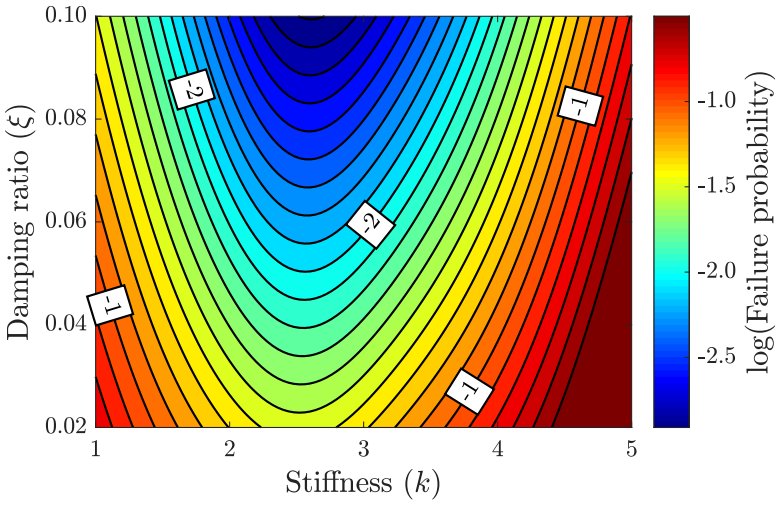

Figure 5: Iso-probability curves. Example No.1: Second scenario

The samples obtained during the different stages of the proposed design process are shown in Fig. 6. The same setting used in the first scenario, in terms of the number of samples per stage and proposal distribution parameters, is considered here. At the last stage, the samples populate a vicinity of the optimal solution, which is consistent with Fig. 5. Note that the results of Fig. 5 have been validated by means of an exhaustive evaluation of all available values of the stiffness parameter.

The trend of the objective function values obtaining during the different stages is shown in Fig. 7. At the last stage, the failure probability ranges from 5.50×10^{-4} to 5.58×10^{-4}. The optimal design is given by $k = 2.6$ and $\xi = 0.099$ (sample-based optimum design), with associated probability of failure equal to 5.50×10^{-4} (sample-based optimal solution). To get more insight

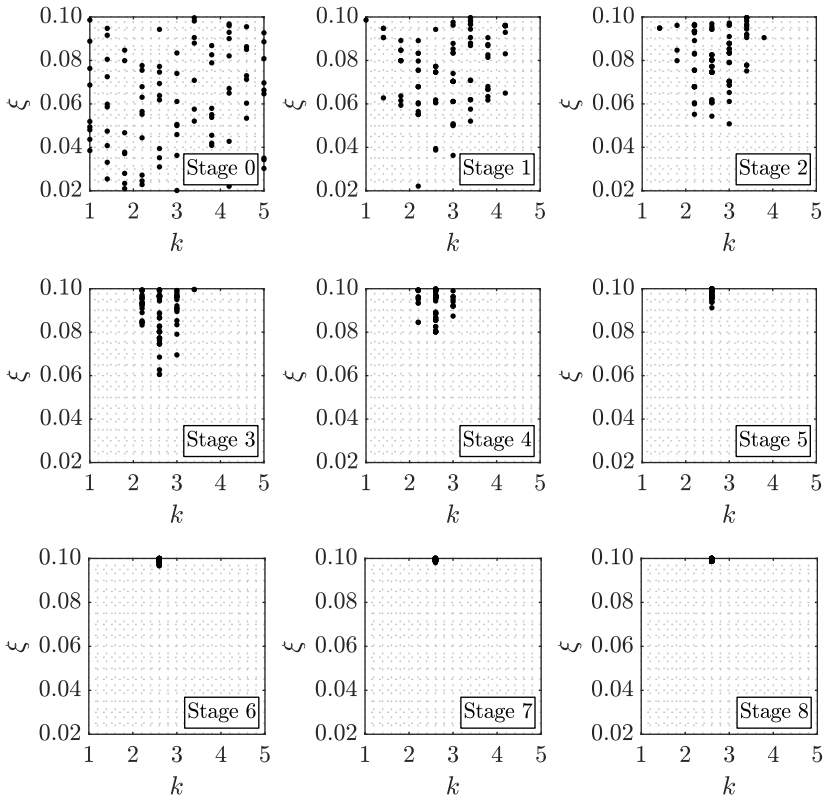

Figure 6: Evolution of samples during different stages. Example No.1: Second scenario

into the updating process, the normalized coefficient of variation of the objective function values during the different stages is shown in Fig. 8 (see Appendix B). It is observed that the sample coefficient of variation decreases with the number of stages reaching a value close to 0.1% of the initial coefficient of variation of the objective function values at the last stage. This small value explains the fact that the failure probability estimates are very similar at the different designs obtained at last stage (see Fig. 7). In addition, it is clear that the optimization scheme reaches the optimal solution. That is, all samples are concentrated around the global optimal solution, as previously pointed out.

Finally, Table 2 shows the statistical performance of the optimization scheme based on 30 independent runs of the updating process, with the number of samples n used in one stage ranging from 10 to 200. As in the previous scenario, the best, the mean, and the worst solutions across the different optimization runs are obtained in terms of the system failure probability. It is seen that these values show a very small variation when $n \geq 50$. Similarly, the corresponding coefficient of variation (c.o.v.) of the minimum failure probability values reduces as n increases. In other words, the optimization scheme is insensitive to n with respect to the optimum design when $n \geq 50$. Thus,

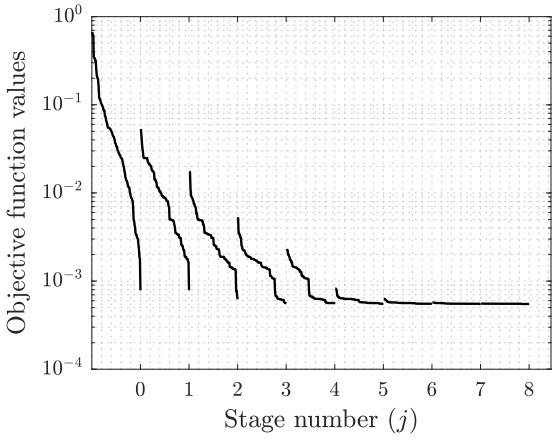

Figure 7: Objective function values obtained during the updating process. Example No.1: Second scenario

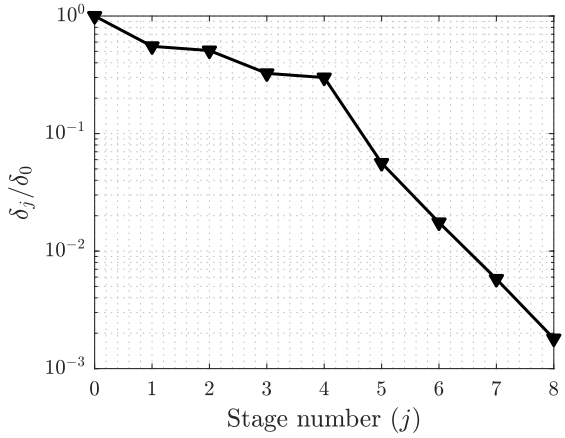

Figure 8: Evolution of the normalized coefficient of variation of the objective function values during the different stages. Example No.1: Second scenario

n	best	mean	worst	c.o.v.
10	5.50×10^{-4}	5.72×10^{-4}	7.79×10^{-4}	9.0×10^{-2}
25	5.50×10^{-4}	5.55×10^{-4}	5.70×10^{-4}	9.0×10^{-3}
50	5.50×10^{-4}	5.51×10^{-4}	5.56×10^{-4}	4.0×10^{-3}
100	5.50×10^{-4}	5.50×10^{-4}	5.52×10^{-4}	2.0×10^{-3}
200	5.50×10^{-4}	5.50×10^{-4}	5.51×10^{-4}	0.3×10^{-3}

Table 2: Statistical performance of proposed scheme. Example No.1: Second scenario

even with a relatively small number of samples per stage the algorithm is capable to explore the design space in a very effective manner.

8.2. Example No. 2

8.2.1. Model Description

The two-story frame structure with friction-based devices under earthquake loading shown in Figure 9 is considered in this example. The floor masses are $m_i = 10^7$ kg, $i = 1, 2$, and the linear interstory stiffnesses are denoted by k_1 and k_2. In addition, a 5% of critical damping is assumed in the model. For an improved earthquake resistance, the structure is reinforced with a friction-based device at each floor. The devices follow the inter-story restoring force law $\kappa(t) = k_d\Big(\delta(t) - \eta^1(t) + \eta^2(t)\Big)$, where k_d denotes the initial stiffness of the device, $\delta(t)$ is the relative displacement between floors, and $\eta^1(t)$ and $\eta^2(t)$ denote the plastic elongations of the device. Using the auxiliary variable $\mu(t) = \delta(t) - \eta^1(t) + \eta^2(t)$, the plastic elongations $\eta^1(t)$ and $\eta^2(t)$ are specified by the differential equations [54]

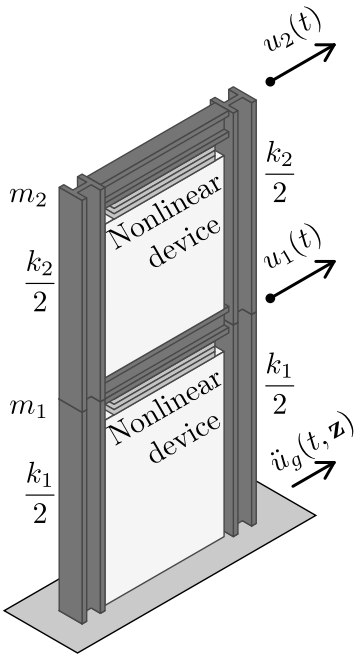

Figure 9: Two-degree-of-freedom system.

$$\dot{\eta}^1(t) = \dot{\delta}(t)H(\dot{\delta}(t)) \times \Big[H(\mu(t) - \mu_y)\frac{\mu(t) - \mu_y}{\mu_p - \mu_y}H(\mu_p - \mu(t)) + H(\mu(t) - \mu_p)\Big] \tag{32}$$

and

$$\dot{\eta}^2(t) = -\dot{\delta}(t)H(-\dot{\delta}(t)) \times \Big[H(-\mu(t) - \mu_y)\frac{-\mu(t) - \mu_y}{\mu_p - \mu_y}H(\mu_p + \mu(t)) + H(-\mu(t) - \mu_p)\Big] \tag{33}$$

where $H(\cdot)$ denotes the Heaviside step function, μ_y is a parameter specifying the onset of yielding, and $k_d\ \mu_p$ is the maximum restoring force of the device. The values $\mu_p = 6.0 \times 10^{-3}$ m, $\mu_y = 0.7 u_p$, and $k_d = 6.0 \times 10^8$N/m are used for the nonlinear elements. Note that because of yielding, energy dissipation due to hysteresis is introduced in the structural response. It is noted that even though the nonlinear model is relatively simple from a structural point of view, different levels of interaction between the design variables may be obtained.

8.2.2. Stochastic Excitation

The system is subjected to a ground acceleration that is modeled as a non-stationary filtered white noise process. Specifically, the ground acceleration is defined as $\ddot{u}_g(t) = \Omega_1^2 w_1(t) + 2\xi_1\Omega_1 w_2(t) - \Omega_2^2 w_3(t) - 2\xi_2\Omega_2 w_4(t)$, where the filter state variables $w_i, i = 1, 2, 3, 4$, satisfy the differential equation

$$\frac{d}{dt}\begin{Bmatrix} w_1(t) \\ w_2(t) \\ w_3(t) \\ w_4(t) \end{Bmatrix} = \begin{bmatrix} 0 & 1 & 0 & 0 \\ -\Omega_1^2 & -2\xi_1\Omega_1 & 0 & 0 \\ 0 & 0 & 0 & 1 \\ \Omega_1^2 & 2\xi_1\Omega_1 & -\Omega_2^2 & -2\xi_2\Omega_2 \end{bmatrix} \begin{Bmatrix} w_1(t) \\ w_2(t) \\ w_3(t) \\ w_4(t) \end{Bmatrix} + \begin{Bmatrix} 0 \\ \omega(t)e(t) \\ 0 \\ 0 \end{Bmatrix} \tag{34}$$

where $\omega(t)$ denotes white noise, and $e(t)$ is an envelope function. The envelope function is taken of the form $e(t) = (e^{-0.5t} - e^{-t})/\max_{t^* \in [0,t_T]}(e^{-0.5t^*} - e^{-t^*})$. The values $\Omega_1 = 15.0$ rad/s, $\xi_1 = 0.6$, $\Omega_2 = 1.0$ rad/s, and $\xi_2 = 0.9$, and white noise intensity $I = 0.036$ m^2/s^3 are used in this example. For numerical implementation, the sampling interval and the duration of the excitation are taken as $\Delta t = 0.01$s, and $t_T = 10$s, respectively. Moreover, a discrete-time white noise sequence $\omega(t_j) = \sqrt{I/\Delta t}\ z_j$, where $z_j, j = 1, \ldots, 1001$, are independent identically distributed standard Gaussian random variables, is considered. Note that a total of 1001 random variables are involved in the characterization of the excitation. Thus, the vector of uncertain parameters $\mathbf{z}$ involved in the problem is high-dimensional.

8.2.3. Design Problem

The objective of this example problem is to perform a reliability-based design of the two-story frame structure with respect to the linear interstory stiffnesses k_1 and k_2. The objective function is defined in terms of an initial cost which is assumed to be proportional to the linear interstory stiffnesses. Two reliability constraints are considered. The first constraint is related to a failure

event associated with the lateral displacement of the first floor, while the second constraint is associated with the lateral displacement of the second floor. Thus, the corresponding demand functions are given by

$$d_j(\mathbf{x}, \mathbf{z}) = \max_{t\in[0,t_T]}\{\mid u_j(t, \mathbf{x}, \mathbf{z}) \mid /u_j^*\} \quad , \quad j = 1, 2 \tag{35}$$

where $\mathbf{x} = \langle k_1, k_2\rangle^T$ is the vector of design variables, $u_j(t, \mathbf{x}, \mathbf{z})$ is the lateral displacement of the j^{th} floor, and $u_j^*, j = 1, 2$ are the acceptable response levels equal to $u_1^* = 0.015$m, and $u_2^* = 0.03$m. In addition, a geometric design requirement in terms of the design variables is also considered, i.e., $k_2 \leq k_1$. A pure discrete variable treatment of the problem is considered in this case. The optimization problem is written as

$$\begin{aligned} \text{Min}_{(k_1,k_2)} \quad & f(k_1, k_2) \ = (c/10^{10})\ (k_1 + k_2) \\ s.t. \quad & P_{F_j}(k_1, k_2) \leq 10^{-4} \quad , \quad j = 1, 2 \\ & k_2/k_1 \leq 1 \\ & k_j \in \mathbf{K}_j \quad , \quad j = 1, 2 \end{aligned} \tag{36}$$

where $(c/10^{10})$ is a cost factor, $P_{F_j}(k_1, k_2)$ is the failure probability function associated with the failure event characterized by the demand function d_j, and the sets of available discrete values for the design variables are given by

$$\mathbf{K}_1 = \mathbf{K}_2 = \{0.3 + 0.01j, j = 0, \ldots, 90\}\ 10^{10}\text{N/m} \tag{37}$$

Note that the previous setting leads to 91 available options for each design variable, leading to a total of more than 8,000 possible designs. The linear interstory stiffnesses can take values between 0.3×10^{10}N/m and 1.2×10^{10}N/m.

8.2.4. Results

The iso-probability curves associated with the failure events related to the lateral displacements of the first and second floor are shown in Fig. 10. As in the previous example, the smoothed curves are shown in the continuous design space and they are constructed by using a set of failure probability estimates distributed over the design space. It is observed that the failure probability

related to the displacement of the first floor depends mainly on the first interstory stiffness and a small interaction with the second interstory stiffness is observed. Contrarily, the interaction between the design variables is clear for the failure probability associated with the displacement of the second floor. These results are reasonable from an engineering viewpoint.

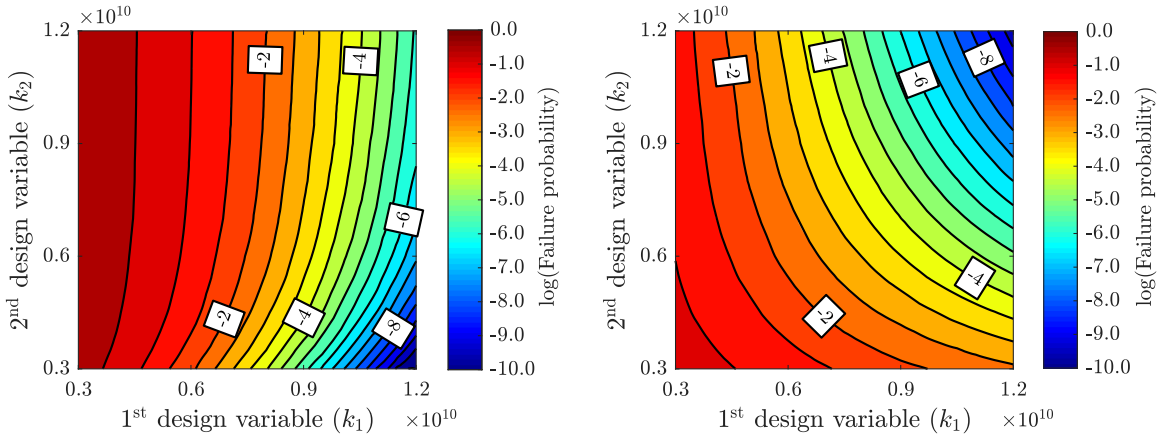

Figure 10: Iso-probability curves. Left figure: failure event related to the lateral displacement of the first floor. Right figure: failure event related to the lateral displacement of the second floor.

A sketch of the corresponding feasible design space of the optimization problem in the continuous and discrete spaces is presented in Fig. 11, where some contour curves of the objective function are also shown. From a practical point of view, it is seen that the optimal solution set $\mathbf{X}_f^*$ can be defined in terms of the five designs marked by red dots in the right figure of Fig. 11, that is, $\mathbf{X}_f^* = \{\langle 0.98, 0.63\rangle^T, \langle 0.99, 0.62\rangle^T, \langle 1.00, 0.61\rangle^T, \langle 1.01, 0.60\rangle^T, \langle 1.02, 0.59\rangle^T\} \times 10^{10}\text{N/m}$, with optimum normalized objective function value equal to $f = 1.61$. These results have been validated by means of an exhaustive evaluation of all available designs.

The set of feasible samples uniformly distributed over the feasible design space is shown in Fig.12 (Stage 0). These samples are obtained after four stages of the proposed procedure for obtaining samples in the feasible design space. To this end, and for illustration purposes, the algorithm is implemented by considering 100 samples per stage. The distribution parameters of the proposal distributions for the discrete design variables are set equal to $\lambda_l^* = 10, l = 1, 2$, and $\tau = 0.05$. Note that with this selection of λ_l^*, the maximum number of discrete values adjacent to a lead sample is equal to 21, including the lead sample. This number is about 20% of the available discrete values for the design variables, and therefore this value defines a somewhat medium-size support for the proposal distributions. This is done in order to explore the entire feasible design space in an effective manner. In fact, almost 100 different feasible designs are generated in four

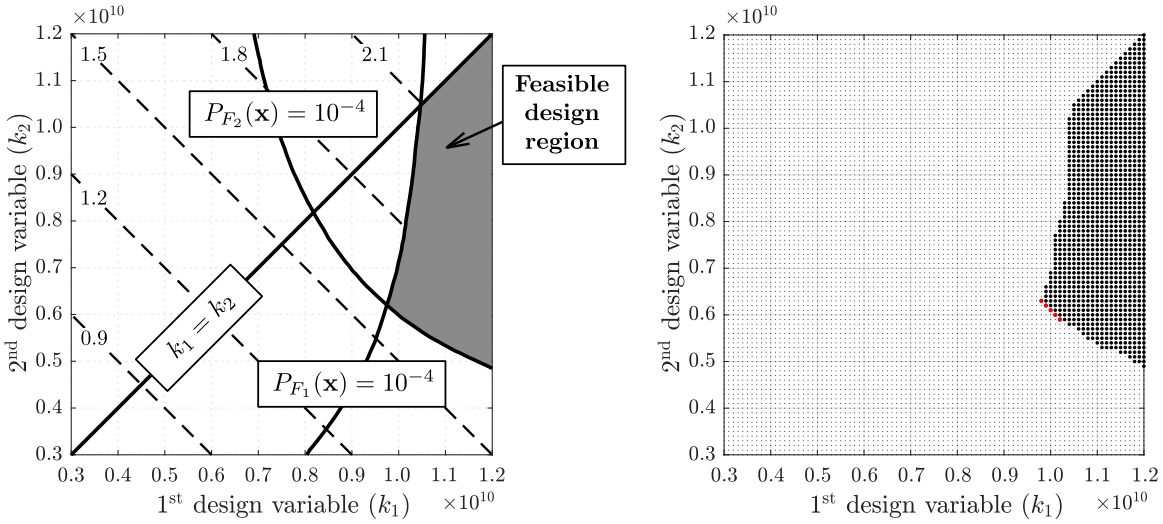

Figure 11: Sketch of the feasible design space. Left figure: feasible design space and some contour curves of the objective function in the continuous design space. Right figure: feasible design space in the discrete design space. Unfeasible designs (white dots). Feasible designs (black dots). Optimal designs (red dots).

stages. Note that the shape generated by these samples resembles the feasible design space shown in Fig. 11. The designs obtained from the first five stages of the procedure outlined in Sections 3.3 and 4.3 for generating samples distributed in the vicinity of the optimal solution set are also shown in Fig. 12. The number of samples per stage is also set equal to 100. The distribution parameters of the proposal distributions are set equal to $\lambda_l^* = 5, l = 1, 2$, and $\tau = 0$ for this step of the process. Note that this choice of λ_l^* results in proposal distributions with smaller supports than the ones used in the procedure for obtaining samples in the feasible design space. Thus, the algorithm favors samples in the vicinity of the current state. Numerical results show that this selection is appropriate in the sense that the proposed scheme converges to the target optimal solution set in an efficient manner. At the last stage, the samples populate a vicinity of the optimal solution set, which is consistent with Figure 11. In other words, all samples at the last stage are in the vicinity of the optimal solution set.

The maximum and minimum normalized objective function values obtained during the different stages are shown in Figure 13. It is seen that from stage number four, the maximum and minimum values are almost coincident. Actually, the minimum normalized objective function value obtained during the simulation process (sample-based optimum cost) is equal to 1.61, which is obtained at the following sample-based optimal designs: $\langle 0.98, 0.63\rangle^T \times 10^{10}$N/m; $\langle 0.99, 0.62\rangle^T \times 10^{10}$N/m; $\langle 1.00, 0.61\rangle^T \times 10^{10}$N/m; $\langle 1.01, 0.60\rangle^T \times 10^{10}$N/m; and $\langle 1.02, 0.59\rangle^T \times 10^{10}$N/m. Thus, the scheme

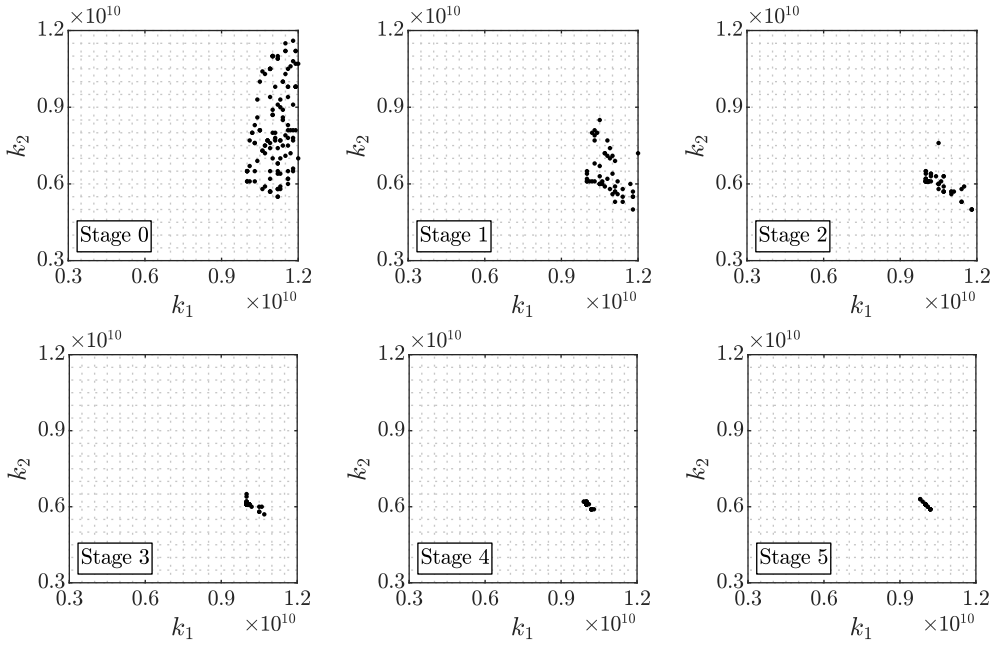

Figure 12: Evolution of samples during different stages of the proposed procedure for obtaining samples in the optimal solution set

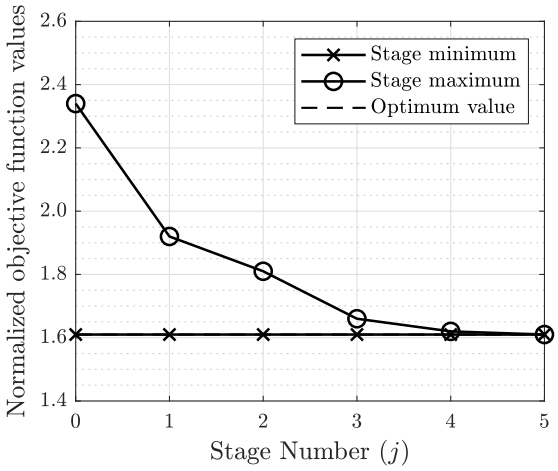

Figure 13: Maximum and minimum normalized objective function values obtained during the different stages.

is able to identify the designs that define the optimal solutions in this particular run. Moreover, information about the value of the reliability constraints at the optimal designs is given in Table 3. Considering the variability of the reliability estimates, it is observed that from a practical viewpoint the reliability constraints $P_{F_1}(k_1, k_2) \leq 10^{-4}$ and $P_{F_2}(k_1, k_2) \leq 10^{-4}$ are active at the optimal design $k_1 = 0.98 \times 10^{10}\text{N/m}, k_2 = 0.63 \times 10^{10}\text{N/m}$, while the reliability constraint $P_{F_2}(k_1, k_2) \leq 10^{-4}$ is active at the other optimal designs. Note that these results are compatible with the information provided by Fig. 11, which have been corroborated with a comprehensive

assessment of all available designs.

$k_1(10^{10}\text{N/m})$	$k_2(10^{10}\text{N/m})$	$P_{F_1}(k_1,k_2)/10^{-4}$	$P_{F_2}(k_1,k_2)/10^{-4}$
0.98	0.63	0.95	0.94
0.99	0.62	0.65	0.94
1.00	0.61	0.43	0.93
1.01	0.60	0.31	0.94
1.02	0.59	0.22	0.99

Table 3: Reliability constraint values at the optimal designs.

A study about the statistical performance of the design scheme based on 200 independent runs indicates that the scheme performs in an effective manner when the number of samples per stage n is greater than a value around 50. Actually, when $n \geq 50$ all samples concentrate around the optimal solution at the last stage of the scheme. Moreover, in 99% of the cases, at least one design in the optimal solution set $\mathbf{X}_f^*$ is identified. In other words, the algorithm is capable to explore the discrete design space in a very effective manner with a relatively small number of samples per stage. Based on the previous information, the total number of function evaluations during the entire optimization process is less than 400 in this case. This small number of function calls indicates that the proposed scheme is quite effective in terms of computational cost.

8.2.5. Effect of Nonlinear Devices

The effect of the friction-based devices on the final design is next investigated. In particular, the influence of the initial stiffness of the devices, k_d, on the final design is studied. Figure 14 shows samples in the feasible design space for the case of three different values of k_d, namely, $k_d = 0.0$ (Case-A), $k_d = 6.0\times10^8$N/m (Case-B), and $k_d = 12.0\times10^8$N/m (Case-C). For illustration purposes, about 200 feasible samples are shown in each case.

Note that Case-A ($k_d = 0.0$) corresponds to a linear model, that is, the structure without the friction-based devices. On the other hand, Case-C can be interpreted as a device stiffer than the device used in the example, that is, Case-B. It is observed that the effect of this parameter is significant. An increase of the device initial stiffness increases the size of the feasible design space. This is reasonable since the model becomes stiffer and therefore designs which are more flexible, in terms of the linear interstory stiffnesses, also satisfy the reliability constraints. The corresponding

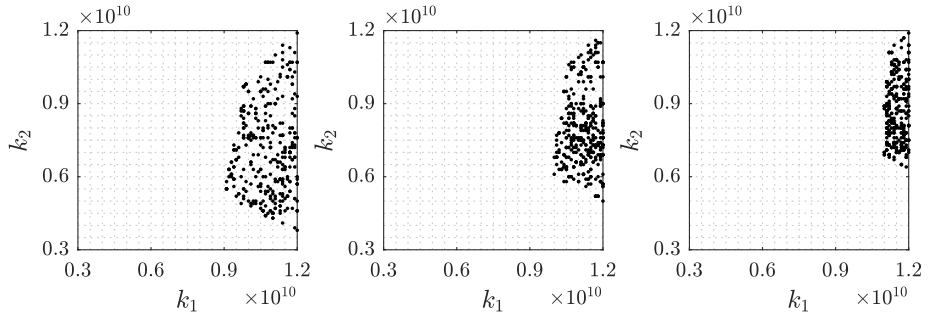

Figure 14: Samples uniformly distributed over the feasible design space. Left figure: $k_d = 12.0 \times 10^8$N/m. Middle figure: $k_d = 6.0 \times 10^8$N/m. Right figure: $k_d = 0.0$.

optimal normalized objective function values are given in Table 4.

$k_d(10^8\text{N/m})$ initial stiffness	normalized objective function value
0.0 (Case-A)	1.79
6.0 (Case-B)	1.61
12.0 (Case-C)	1.43

Table 4: Objective function values at final designs.

Note that an increase of the device initial stiffness decreases the objective function values. In other words, the linear structure at the final design is more flexible, or equivalently, the dimension of the structural columns decreases as the initial stiffness of the devices increases. This is due to the fact that the nonlinear devices provide additional stiffness to the model, as previously pointed out. Comparing Case-A with Case-C, it is observed that the objective function value corresponding to the linear model is almost 25% higher than the objective function value corresponding to the nonlinear model characterized by $k_d = 12.0 \times 10^8$N/m. Thus, the effect of the nonlinear devices is quite beneficial in terms of the final design from this point of view.

8.3. Example No. 3

8.3.1. Description of the Model

The structural model shown in Figure 15 is considered as an application problem. The system is subjected to a ground acceleration modeled as in the first example problem, where the duration of the excitation is taken as $t_T = 15$s. Thus, more than 1500 random variables are involved in the characterization of the stochastic excitation in this case. Each floor is supported by 48 columns

as shown in Fig. 15. The axes A, C, D, and F contribute mainly to the horizontal resistance of the floors in the x direction. On the contrary, the resistant axes B and E work primarily in the y direction. All floors have a constant height equal to 3.2 m, leading to a total height of 12.8 m. For a given floor, all columns are assumed to be equal and their specifications are given in Table 5 [55].

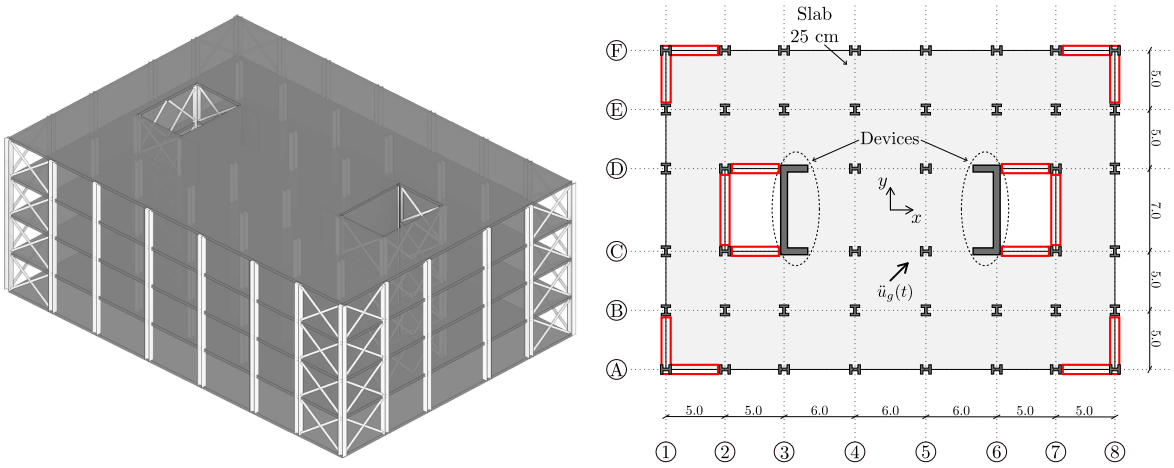

Figure 15: Isometric and plan view of the structural model.

Floor	Type of section
1	W24 × 131
2	W24 × 131
3	W24 × 104
4	W24 × 104

Table 5: Specification of column elements.

In addition, a bracing system is considered in the model. Specifically, tubular steel brace elements are placed in axes A, C, D and F (acting in the x direction), and in axes 1, 2, 7 and 8 (acting in the y direction). In axes A, C, D, F, 1, and 8 two brace systems are placed, while one brace system is placed in axes 2 and 7. A typical configuration of the brace elements is shown in Fig. 16. Thus, a total of 128 brace elements are used in the model, with material properties $E = 2.1 \times 10^{11}$ N/m^2, and weight density $\rho = 7.42$ ton/m^3.

From the modeling viewpoint, it is assumed that each floor may be represented sufficiently accurate as rigid within the $x - y$ plane when compared with the flexibility of the horizontal

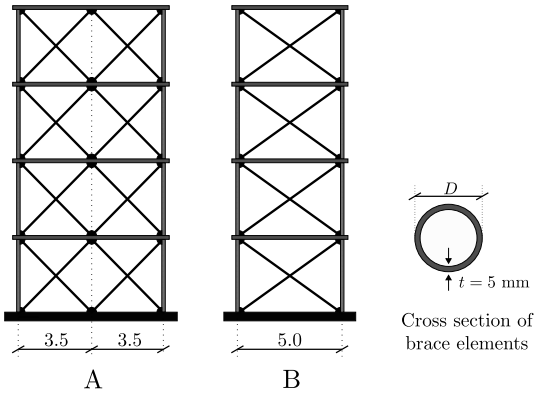

Figure 16: Typical configuration of brace elements. A). Brace system in axes 2 and 7. B) Brace system in axes A, C, D, F, 1, and 8.

resistance elements. Hence, each floor can be represented by three degrees of freedom, i.e. two translatory displacements in the direction of the x and y axes, and a rotational displacement about the z axis. The associated masses $m_x = m_y$ and m_z are taken as constant for all floors and equal to 5.98×10^5 kg, and 1.10×10^8 kg m^2, respectively. In addition, a 2% of critical damping is assumed in the model. For aseismic design purposes, the model is reinforced with friction-based devices at each floor. At each floor, six devices are implemented as shown in the floor plan of the model. Specifically, four devices in the x direction and two devices in the y direction are considered. These elements provide additional resistance against relative displacements between floors. The devices follow the inter-story restoring force law described in Example No. 2 (see Section 8.2.1). The restoring force of the devices acts between the adjacent floors with the same orientation of the devices.

8.3.2. Optimization Problem

The objective function for the optimization problem is defined in terms of total volume associated with the brace elements. The vector of design variables $\mathbf{x}$ is defined in terms of the areas of the cross-sections of the steel brace elements. The available discrete values for the design variables (areas of tubular cross-sections) are presented in Table 5. Each of the design variables can be chosen from a discrete set of 48 tubular elements. Two failure events are considered. They are defined in terms of the maximum roof displacement (in the x or y direction), and the maximum axial stress of the brace elements. The related demand functions are given by

D (in)	A (mm^2)	D (in)	A (mm^2)	D (in)	A (mm^2)
2	719	4	1517	6	2315
2 1/8	769	4 1/8	1567	6 1/8	2365
2 1/4	819	4 1/4	1617	6 1/4	2415
2 3/8	869	4 3/8	1667	6 3/8	2465
2 1/2	919	4 1/2	1717	6 1/2	2515
2 5/8	969	4 5/8	1767	6 5/8	2565
2 3/4	1019	4 3/4	1817	6 3/4	2615
2 7/8	1069	4 7/8	1866	6 7/8	2664
3	1118	5	1916	7	2714
3 1/8	1168	5 1/8	1966	7 1/8	2764
3 1/4	1218	5 1/4	2016	7 1/4	2814
3 3/8	1268	5 3/8	2066	7 3/8	2864
3 1/2	1318	5 1/2	2116	7 1/2	2914
3 5/8	1368	5 5/8	2166	7 5/8	2964
3 3/4	1418	5 3/4	2216	7 3/4	3014
3 7/8	1468	5 7/8	2265	7 7/8	3063

Table 6: Available values for the design variables

$$d_1(\mathbf{x},\mathbf{z}) = \max_{t\in[0,t_T]}\{\mid u_r(t,\mathbf{x},\mathbf{z}) \mid /u_r^*\}$$
$$d_2(\mathbf{x},\mathbf{z}) = \max_{i=1,\ldots,128}\max_{t\in[0,t_T]}\{\mid \sigma_i(t,\mathbf{x},\mathbf{z}) \mid /\sigma^*\} \tag{38}$$

where $u_r(t,\mathbf{x},\mathbf{z})$ is the roof displacement in the x or y direction, $\sigma_i(t,\mathbf{x},\mathbf{z})$ is the axial stress of the i^{th} brace element, and u_r^* and σ^* are the acceptable response levels equal to $u_r^* = 0.033$m, and $\sigma^* = 3.31 \times 10^8$Pa (80% of yield stress).

8.3.3. Results: Case of Two-Linked Design Variables

Two design variables are first considered in order to get insight into the optimization problem. Design variable number one (x_1) represents the area of the brace elements acting in the x direction, while the second design variable (x_2) controls the brace elements acting in the y direction. The design problem is written as

$$
\begin{aligned}
\text{Min}_{\mathbf{x}} \quad & f(\mathbf{x}) \;=\; \sum_{i=1}^{2} c_i \, x_i \\
s.t. \quad & P_{F_j}(\mathbf{x}) \leq 5.0 \times 10^{-4} \;,\; j = 1, 2 \\
& x_j \in \mathbf{X} \;\;,\;\; j = 1, 2
\end{aligned} \tag{39}
$$

where $\mathbf{x} = \langle x_1, x_2 \rangle^T$ is the vector of design variables, c_1 and c_2 are normalization constants and equal to $c_1 = 1.7 \times 10^{-4}$, $c_2 = 1.55 \times 10^{-4}$, $P_{F_j}(\mathbf{x})$ is the failure probability function associated with the failure event characterized by the demand function d_j, and $\mathbf{X}$ represents the set of available discrete values for the design variables given in Table 6. Note that there are 2304 possible designs in this case. As in the previous examples, the reliability estimation for a given design constitutes a high-dimensional problem.

For illustration purposes, the smoothed iso-probability curves associated with the failure events related to the roof displacement and maximum axial stress of the brace elements are presented in Fig. 17. Moreover, a sketch of the feasible design space in the continuous and discrete spaces is shown in Fig. 18. A strong interaction between the design variables is observed for the failure probabilities associated with both failure events especially for stiff brace systems. This is due to the type of response functions considered in the definition of the failure events and the relative complexity of the structural model.

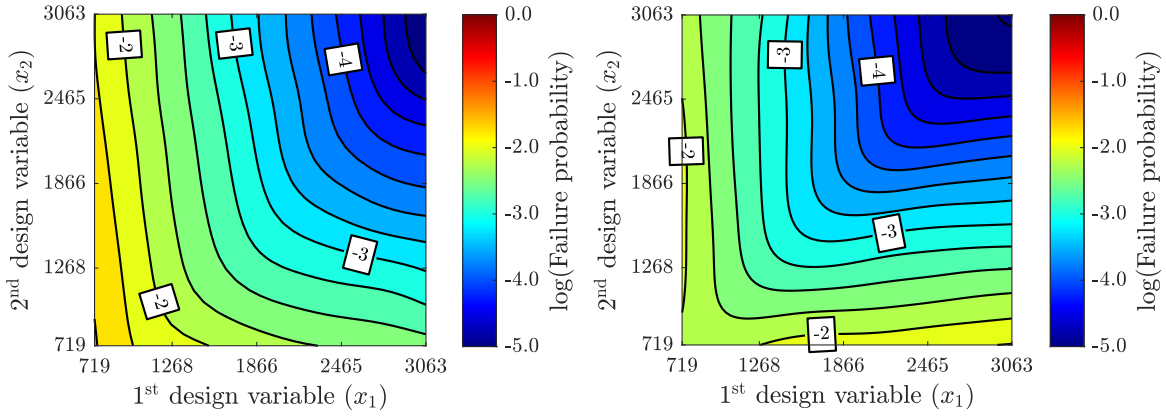

Figure 17: Left Figure: Iso-probability curves associated with the failure event related to the roof displacement. Right Figure: Iso-probability curves associated with the failure event related to the maximum axial stress of the brace elements.

A statistical performance assessment of the proposed design scheme indicates that the scheme performs in an effective manner when the number of samples per stage n is such that $n \geq 50$. The

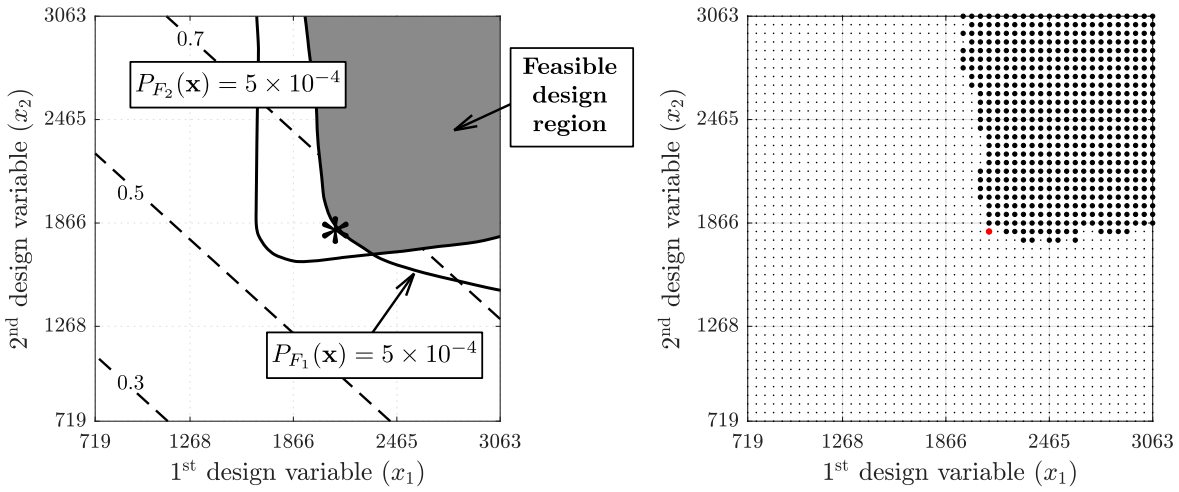

Figure 18: Sketch of the feasible design space. Left figure: feasible design space and some contour curves of the objective function in the continuous design space. Right figure: feasible design space in the discrete design space. Unfeasible designs (white dots). Feasible designs (black dots). Optimal design (red dot).

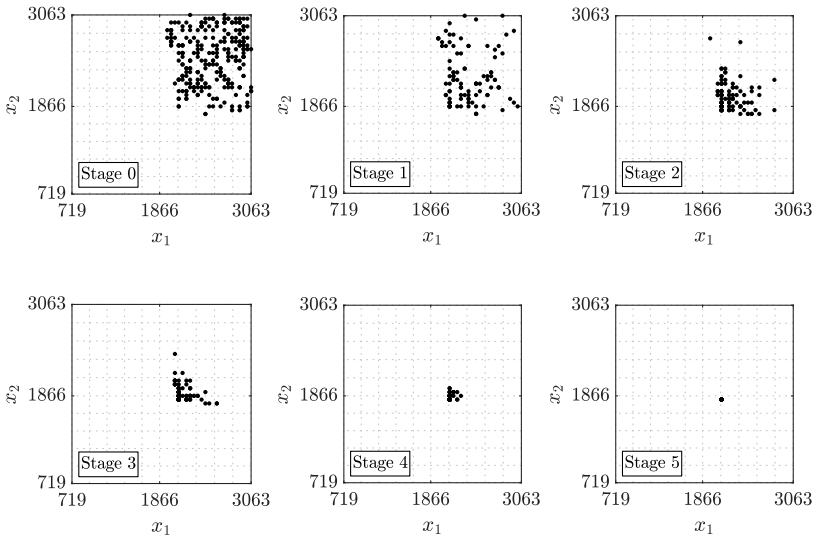

Figure 19: Evolution of samples during different stages of the proposed procedure for obtaining samples in the optimal solution set

corresponding set of feasible samples uniformly distributed over the feasible design space is shown in Fig. 19 (Stage 0). These samples are obtained after three stages of the proposed procedure for obtaining samples in the feasible design space. The algorithm is implemented with distribution parameters of the proposal distributions for the discrete design variables equal to $\lambda_l^* = 5, l = 1, 2$, and $\tau = 0.05$. The shape generated by these samples is similar to the feasible design space shown in Fig. 18. The designs obtained from the first five stages of the proposed procedure for generating samples distributed in the vicinity of the optimal solution set are also shown in Fig.

19. At the last stage of the process, the samples populate a vicinity of the optimal solution set, which is consistent with Figure 18. For this step of the process, the distribution parameters of the proposal distributions are equal to $\lambda_l^* = 3, l = 1, 2$, and $\tau = 0$. The optimal design is given by $x_1 = 2116\text{mm}^2$, and $x_2 = 1817\text{mm}^2$ (sample-based optimum design), with minimum normalized objective function value (sample-based minimum weight) equal to 0.644. The associated failure probabilities at the sample-based optimal solution are such that $P_{F_1}(x_1, x_2)/5.0 \times 10^{-4} = 0.996$ and $P_{F_2}(x_1, x_2)/5.0 \times 10^{-4} = 0.57$. Then, the reliability constraint $P_{F_1}(x_1, x_2) \leq 5.0 \times 10^{-4}$ can be considered, from the practical viewpoint, active at the final design. These results are compatible with the information provided by Fig. 18, which is based on an exhaustive evaluation of all available designs. Thus, the sample-based optimum obtained by the proposed approach is, in fact, the global optimum. The total number of function evaluations during the entire optimization process is around 400. This number of function calls, which is relatively small in the context of stochastic optimization algorithms, indicates that the scheme is very effective.

8.3.4. Results: Case of Four-Linked Design Variables

As in the previous case, the design variables are the areas of the cross-sections of the steel brace elements. The brace elements located every two floors are linked to two design variables, one associated with the x direction and the other one related to the y direction. Specifically, x_1 and x_3 are associated with the brace elements pointing in the x direction, while x_2 and x_4 with the brace elements pointing in the y direction. The axes and stories corresponding to each design variable are given in Table 7. Note that in this case there are more than 5×10^6 available options for the possible designs.

Design variables	Stories	Axes
x_1	1-2	A C D F
x_2	1-2	1 2 7 8
x_3	3-4	A C D F
x_4	3-4	1 2 7 8

Table 7: Design variables.

The samples uniformly distributed over the feasible design space are shown in Fig. 20. This figure shows the two-dimensional projections and marginal distributions of all feasible designs

obtained during four steps of the proposed approach. The algorithm is implemented by considering 100 samples per stage, with distribution parameters of the proposal distributions for the discrete design variables equal to $\lambda_l^* = 5, l = 1, 2, 3, 4$, and $\tau = 0.025$. A total of 250 feasible samples are obtained, among which 200 are distinct. It is seen that the range of the design variables related to the upper floors is larger than the one observed for the lower floors. This result indicates that the system performance tends to be more sensitive to changes in the lower stories' stiffnesses, as expected.

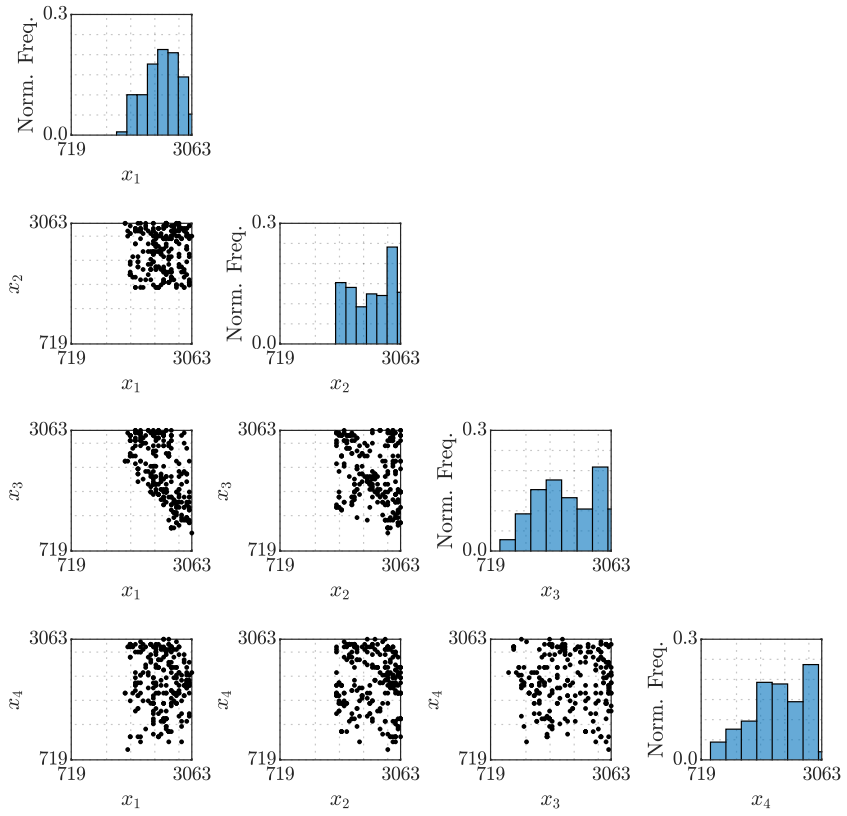

Figure 20: Two-dimensional sample projections and marginal histograms of the feasible samples.

The set of samples obtained after seven stages of the procedure for generating samples distributed in the vicinity of the optimal solution set are shown in Figure 21. It is observed that the samples are concentrated in a very small region of the feasible design space, i.e., almost a single value. For this step of the process, the distribution parameters of the proposal distributions are set equal to $\lambda_l^* = 2, l = 1, 2, 3, 4$, and $\tau = 0$. The maximum and minimum normalized objective function values obtained during the different stages are shown in Figure 22. From stage number seven, the maximum and minimum values are almost coincident. The minimum normalized objective function value obtained during the simulation process (sample-based optimum cost) is

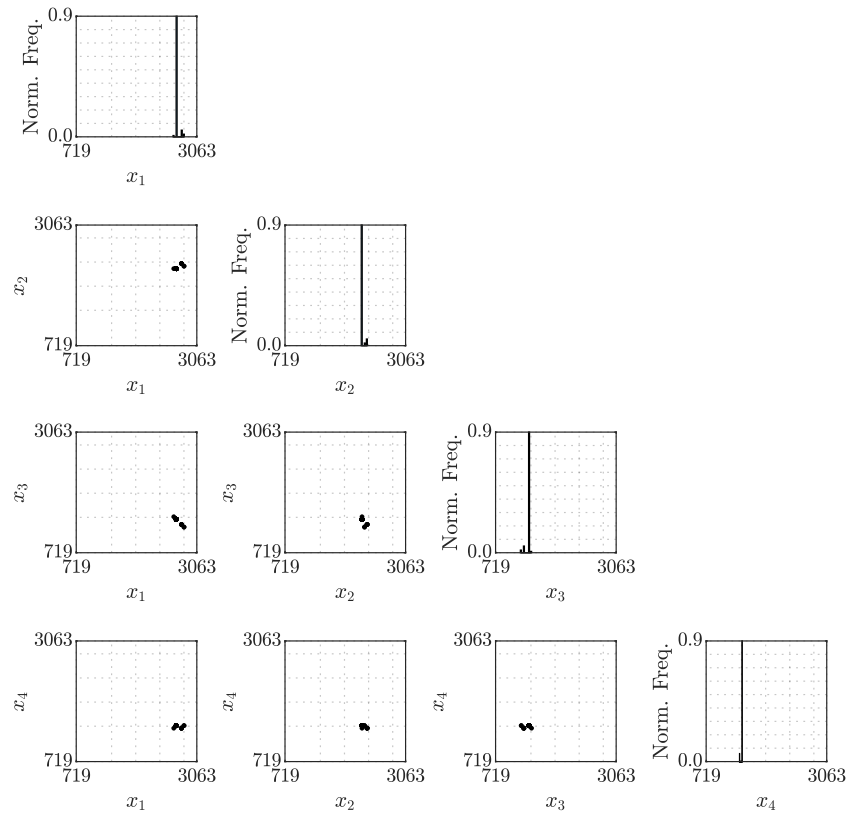

Figure 21: Two-dimensional sample projections and marginal histograms of the design variables in the vicinity of the optimal solution set

equal to 0.6235, which is obtained at the sample-based optimal design given by $x_1 = 2615\text{mm}^2$, $x_2 = 2216\text{mm}^2$, $x_3 = 1418\text{mm}^2$, and $x_4 = 1368\text{mm}^2$. The reliability constraint values at this design are equal to $P_{F_1}(x_1, x_2)/5.0 \times 10^{-4} = 0.994$ and $P_{F_2}(x_1, x_2)/5.0 \times 10^{-4} = 0.0534$. Thus, the reliability constraint $P_{F_1}(x_1, x_2) \leq 5.0 \times 10^{-4}$ can be considered active at the final design, which is compatible with the previous case. It is seen that the final design favors larger values of the optimization variables associated with the brace elements of the lower floors, which is consistent from a structural point of view. Results obtained from other stochastic optimization methods., e.g., genetic algorithms [12], confirm that the sample-based optimal cost obtained by the proposed approach can be regarded as the global solution. Moreover, the analysis shows that alternative designs in the vicinity of the sample-based optimum can also be considered as optimal from the practical viewpoint, given the inherent variability of the failure probability estimates. In this regard, the development of *a posteriori* analysis that reuses information drawn during the optimization process to identify potential new solutions can provide additional flexibility to the overall design process.

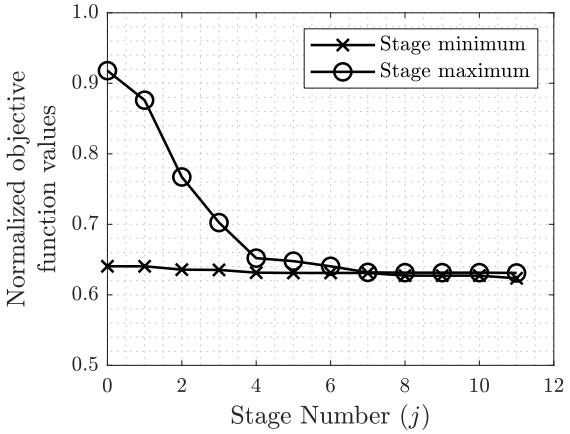

Figure 22: Maximum and minimum normalized objective function values obtained during different stages.

In terms of numerical efforts, the total number of function evaluations is of the order of 1000 in this case. Then, it is seen that the algorithm is capable to obtain the optimal solution set in an effective manner with a relatively small number of samples. Based on the results obtained in the previous examples and additional validation calculations, it is anticipated that the proposed algorithm will compare favorably with respect to other population-based stochastic optimization algorithms for the class of problems considered in the context of this work. An exhaustive comparison of the proposed method with other optimization techniques, in the framework of different mixed discrete-continuous optimization formulations, will be conducted in a future contribution.

9. Conclusions

An approach for solving structural optimization problems considering discrete-continuous design variables has been proposed. The design problem is set into the framework of a Bayesian model updating problem, which is solved by an effective Markov chain Monte Carlo simulation scheme. In particular, the transitional Markov chain Monte carlo method is considered. In the context of the Metropolis-Hastings algorithm, appropriate proposal distributions are suggested for the continuous and discrete design variables. The proposed general formulation is applied to an important class of problems, specifically, reliability-based design optimization of structural systems under stochastic excitation.

Numerical results indicate that feasible samples can be generated in an effective manner even in problems with involved feasible design space geometries. Moreover, the proposed scheme converges to the target optimal solution set in a rather efficient manner. In other words, all samples at the last stage of the process are in the vicinity of the optimal solution set. The samples generated during

the optimization process provide valuable information about the interaction of the design variables. At the same time, they give information about the sensitivity of the final design and constraints with respect to the design variables in the vicinity of the optimal design. This information is quite relevant, specially when dealing with complex structural optimization problems.

Generally, the total number of function evaluations during the entire optimization process is relatively small, indicating that the proposed scheme is quite effective in terms of computational cost. Thus, it is anticipated that the proposed algorithm will compare favorably with respect to other population-based stochastic optimization algorithms. The results of the example problems and additional validation calculations also indicate that, generally, the proposed scheme shows a good performance in terms of its ergodicity. That is, the optimization scheme is able to explore the design space in an effective manner, even with a relatively small number of samples per stage. Nonetheless, as usually observed in the implementation of general stochastic search techniques, the number of function evaluations required to effectively explore the design space might significantly increase for high-dimensional spaces. Based on the preceding observations, it is believed that the proposed design scheme is potentially a useful tool for solving a class of mixed discrete-continuous constrained optimization problems, including problems that deal with stochastic dynamical systems.

A future research effort aims to perform an exhaustive comparison of the proposed method with other stochastic search algorithms in the framework of different mixed discrete-continuous optimization formulations. The consideration of more complex problems in terms of the dimensionality of the design space and the development of specialized techniques to handle them are to follow in the near future. When dealing with problems in which the computational time for evaluating objective and/or constraint functions is significant, the use of meta-models could be very attractive. In this regard, the implementation of the proposed approach by considering an adaptive meta-model for approximating expensive function evaluations during the design process is an additional topic for future research. Besides, the assessment of alternative discrete proposal distributions within the proposed framework is also a future research direction. Work in some of these topics is currently underway.

Acknowledgments

The research reported here was supported in part by CONICYT (National Commission for Scientific and Technological Research) under grant number 1200087. Also, this research has been supported by CONICYT and DAAD under CONICYT-PFCHA/Doctorado Acuerdo Bilateral DAAD Becas Chile/2018-62180007. In addition, this research has been implemented under the PAC (Programa Asistente Cientifico 2017)-UTFSM program. These supports are gratefully acknowledged by the authors.

10. Appendix A

The following schematic flowchart illustrates how the samples in the feasible design space are generated.

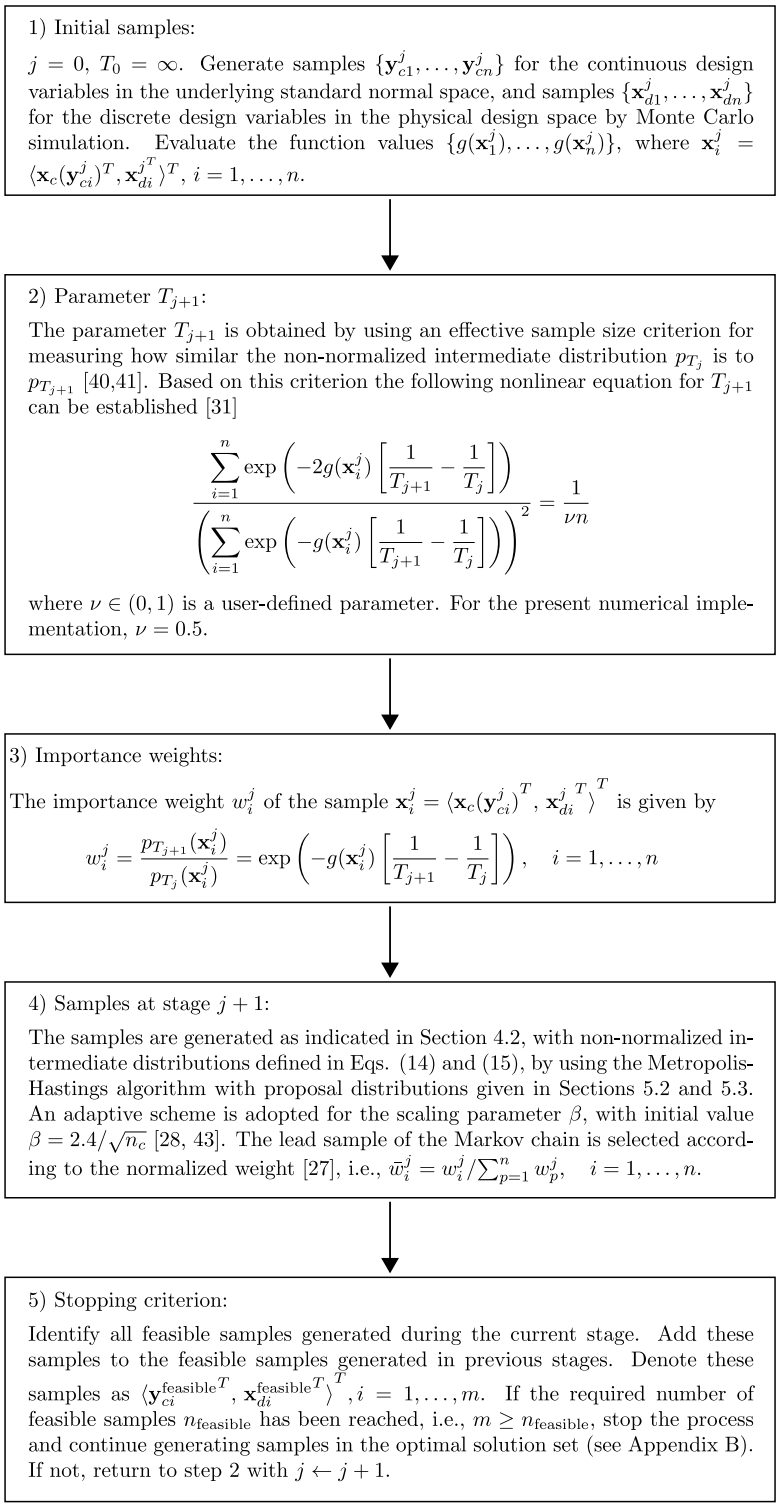

11. Appendix B

The following schematic flowchart illustrates how the samples in the vicinity of the optimal solution space are generated.

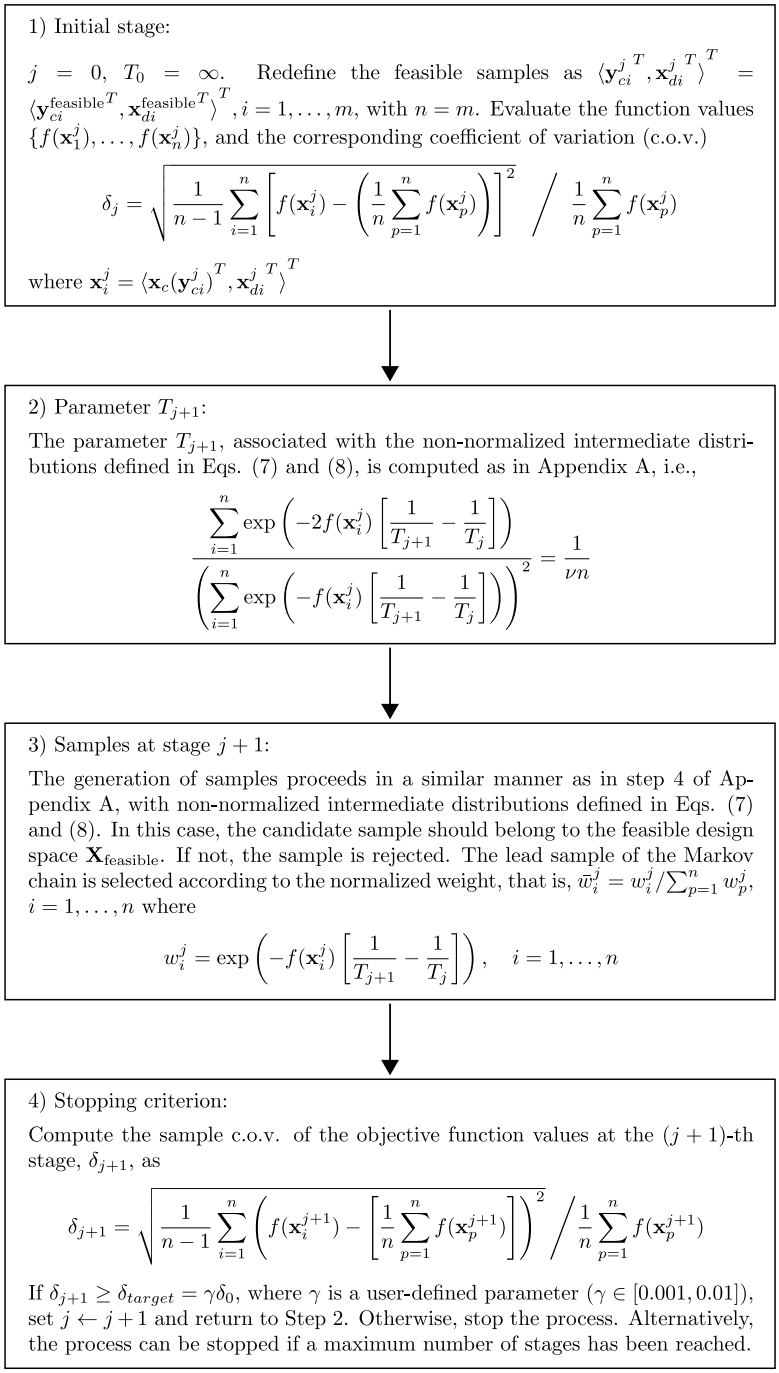

12. References

[1] R.T. Haftka and Z. Gürdal, Elements of Structural Optimization, Third edition, Springer Netherlands, 1992.

[2] M.W. Huang and J.S. Aurora, Optimal design with discrete variables: Some numerical experiments, International Journal for Numerical Methods in Engineering, 40 (1) (1997) 165–188.

[3] J.A. Tomlin, Branch-and-Bound Methods for Integer and Non-convex Programming, J. Abadie (ed.) Elsevier Publishing Co. New York pp. 437-450, 1970.

[4] L.B. Kovács, Combinatorial Methods of Discrete Programming, Mathematical Methods of Operations Research Series, Vol. 2, Akademiai Kiado, Budapest, 1980.

[5] L. Schrage, Integer and Quadratic Programming with LINDO, 4th Edition, The Scientific Press, Redwood City, CA., 1989.

[6] C. Fleury and V. Braibant, Structural optimization: A new dual method using mixed variables, International Journal for Numerical Methods in Engineering, 23(3) (1986) 409–428.

[7] Jensen, H.A. and Beer M. Discrete-continuous variable structural optimization of systems under stochastic loading, Structural and Safety, 32(5) (2010) 293–304.

[8] R. Hassan and W. Crossley, Spacecraft realiability-based design optimization under uncertainty including discrete variables, Journal of Spacecraft and Rockets, 45(2) (2008) 394–405.

[9] H.A. Jensen and J.G. Sepulveda, Structural optimization of uncertain dynamical systems considering mixed-design variables, Probabilistic Engineering Mechanics, 26(2) (2011) 269–280.

[10] C.A. Coello, Discrete optimization of trusses using Genetic Algorithms, in Expert Systems Applications and Artificial Intelligence. J.G. Chen, F.G. Attia and D.L. Crabtree (Eds), I.I.T.T. International, Technology Transfer Series (1994) 331–336.

[11] S. Rajeev and C.S. Krishnamoorthy, Discrete optimization of structures using Genetic Algorithms, Journal of Structural Engineering, 118(5) (1992) 1233–1250.

[12] T.H. Holland, Adaptation in natural and artificial systems, University of Michigan Press, Ann Arbor, Michigan, 2003.

[13] M. Papadrakakis, N.D. Lagaros and V. Plevris, Design optimization of steel structures considering uncertainties, Engineering Structures, 27 (2005) 1408–1418.

[14] S. Kirkpatrick, C.D. Gelatt, M.P. Vecchi, Optimization by simulated annealing, Science, 220(4589) (1983) 165–172.

[15] M. Kripka, Discrete optimization of trusses by simulated annealing, Journal of the Brazilian Soicety of Mechanical Sciences and Engineering, 26(2) (2004) 170–173.

[16] C. Zhang and H.-P. Wang, Mixed-discrete nonlinear optimization with simulated annealing, Engineering Optimization, 21(4) (1993) 277–291.

[17] J. Kennedy and R.C. Eberhart, Particle swarm optimization, in Proc. IEEE Int. Conf. Neural Netw. 4 (1995) 165–172.

[18] C.-J. Liao, C.-T. Tseng and P. Luarn, A discrete version of particle swarm optimization for flowshop scheduling problems, Computers & Operations Research, 34(10) (2007) 3099–3111.

[19] W.-N. Chen, J. Zhang, H. Chung, W.-L. Zhong and Y.-H. Shi, A novel set-based particle swarm optimization method for discrete optimization problems, IEEE Transactions on Evolutionary Computation, 14(2) (2010) 278–300.

[20] C.P. Robert and G. Casella, Monte Carlo statistical methods (2nd ed), Springer, New York, 2004.

[21] C.A. Coello Coello, Theoretical and numerical constraint-handling techniques used with evolutionary algorithms: a survey of the state of the art, Computer Methods in Applied Mechanics and Engineering, 191(11-12) (2002) 1245–1287.

[22] Y. Dong, J. Tang and D. Wang, An application of swarm optimization to nonlinear programming, Computers & Mathematics with Applications, 49(11-12) (2005) 1655-1668.

[23] Z. Michalewicz, Evolutionary algorithms for constrained parameter optimization problems, Evolutionary Computation, 4(1) (1996) 1–32.

[24] A. Hedar and M. Fukushima, Derivative-free filter simulated annealing method for constrained continuous global optimization, Journal of Global Optimization, 35(4) (2006) 521–549.

[25] L.J. Li, Z.B. Huang, F. Liu and Q.H. Wu, A heuristic particle swarm optimizer for optimization of pin connected structures, Computers & Structures, 85(7-8) (2007) 340–349.

[26] H.A. Jensen, D.J. Jerez and M. Beer, A general two-phase Markov chain Monte Carlo approach for design optimization: formulation and applications, submitted to Computer Methods in Applied Mechanics and Engineering.

[27] J. Ching and Y.C. Chen, Transitional Markov chain Monte Carlo method for Bayesian updating, model class selection, and model averaging, Journal of Engineering Mechanics, 133(7) (2007) 816–832.

[28] W. Betz, I. Papaioannou and D. Straub, Transitional Markov chain Monte Carlo: observations and improvements, Journal of Engineering Mechanics, 142(5) (2016) 04016016.

[29] N. Metropolis, A. Resenbluth, M. Resenbluth, A. Teller and E. Teller, Equations of state calculations by fast computing machines, The Journal of Chemical Physics, 21(6) (1953) 1087–1092.

[30] W. Hastings Monte Carlo sampling methods using Markov chains and their applications, Biometrika, 57(1) (1970) 97–109.

[31] K.M. Zuev and J.L. Beck, Global optimization using the asymptotically independent Markov sampling method, Computers and Structures, 126 (2013) 107–119.

[32] J. Wang and L.S. Katafygiotis. Reliability-based optimal design of linear structures subjected to stochastic excitations, Structural Safety, 47 (2014) 29–38.

[33] H.A. Jensen, D.J. Jerez and M. Valdebenito, An adaptive scheme for reliability-based global design optimization: A Markov chain Monte Carlo approach, Mechanical Systems and Signal Processing, 143 (2020) 106836.

[34] J.L. Beck and S.-K. Au, Bayesian updating of structural models and reliability using Markov chain Monte Carlo simulation, Journal of Engineering Mechanics, 128(4) (2002) 380–391.

[35] P. Angelikopoulos, C. Papadimitriou, and P. Koumoutsakos, Bayesian uncertainty quantification and propagation in molecular dynamics simulations: a high performance computing framework, *The Journal of Chemical Physics*, 137(14) (2012) 1441103.

[36] H.A. Jensen, E. Millas, D.Kusanovic and C. Papadimitriou, Model reduction techniques for Bayesian finite element model updating using dynamic response data, *Computer Methods in Applied Mechanics and Engineering*, 279 (2014) 301–324.

[37] J.L. Beck, Bayesian system identification based on probability logic, *Structural Control and Health Monitoring*, 17(7) (2010) 825–847.

[38] E.N. Chatzi and C. Papadimitriou (eds.), Identification Methods for Structural Health Monitoring. Series: CISM-International Centre for Mechanical Sciences, *Springer*, Berlin, Germany, 2016.

[39] K. V. Yuen, Bayesian methods for structural dynamics and civil engineering, *John Wiley & Sons*, 2010.

[40] A. Kong, J. S. Liu and W. H. Wong, Sequential imputations and Bayesian missing data problems, Journal of the American Statistical Association, 89(425) (1994) 278–288.

[41] J. S. Liu, Metropolized independent sampling with comparison to rejection sampling and importance sampling, Statistics and Computing, 6(2) (1996) 113–119.

[42] G. Zanella, Informed proposals for local MCMC in discrete spaces, Journal of the American Statistical Association, (2020) 1–14.

[43] H.A. Jensen, C. Esse, V. Araya and C. Papadimitriou, Implementation of an adaptive meta-model for Bayesian finite element model updating in time domain, Reliability Engineering & System Safety, 160 (2017) 174–190.

[44] J. Li and J. Chen, Stochastic Dynamics of Structures, John Wiley & Sons , Ltd, 2009.

[45] A. Naess, Approximate first-passage and extremes of narrow-band Gaussian and non-Gaussian random vibrations, Journal of Sound and Vibrations, 138 (1990) 365–380.

[46] S.-K. Au and J.L. Beck, Estimation of small failure probabilities in high dimensions by subset simulation, Probabilistic Engineering Mechanics, 16(4) (2001) 263–277.

[47] P.S. Koutsourelakis, H.J. Pradlwarter and G.I. Schuëller, Reliability of structures in high dimensions, part I: Algorithms and applications, Probabilistic Engineering Mechanics, 19(4) (2004) 409–417.

[48] H.J. Pradlwarter, G.I. Schuëller, P.S. Koutsourelakis and D.C. Champris, Application of line sampling simulation method to reliability benchmark problems, Structural Safety, 29(3) (1998) 208–221.

[49] D.M. Moore, Simulation of ground motion using the stochastic method, Pure and Applied Geophysics, 160 (2003) 635–676.

[50] G.M. Atkinson and W. Silva, Stochastic modeling of California ground motions, Bulletin of the Seismological Society of America, 90(2) (2000) 255–274.

[51] J.G. Anderson and S.E. Hough, A model for the shape of the Fourier amplitude spectrum of acceleration at high frequencies, Bulletin of the Seismological Society of America, 74(5) (1984) 1969–1993.

[52] G.P. Mavroeidis, A mathematical representation of near-fault ground motions, Bulletin of the Seismological Society of America, 93(3) (2003) 1099–1131.

[53] S.-K. Au and Y. Wang, Engineering risk assessment with Subset Simulation, John Wiley & Sons Inc., 2014.

[54] H.J. Pradlwarter, G.I. Schuëller and U. Dorka, Reliability of MDOF-systems with hysteretic devices, Engineering Structures, 20(8) (1998) 685–691.

[55] American Institute of Steel Construction, AISC manual of steel construction: load and resistance factor design (3rd ed.), 2001.

[56] S.-K. Au and Y. Wang, Genetic algorithms in search, optimization, and machine learning, Addison-Wesley Publishing Company, 1989.